Journal of Energy Storage 140 (2025) 118847

Contents lists available at ScienceDirect

Journal of Energy Storage

journal homepage: www.elsevier.com/locate/est

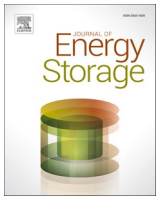

Research papers

Enhanced PSO-based optimisation with probabilistic analysis for standalone DC microgrid design

Hasith Jayasinghe [a,b,*], Kosala Gunawardane [a], Md. Alamgir Hossain [c], Ramon Zamora [d], Mark Anthony Preece [e]

[a] School of Electrical and Data Engineering, Faculty of Engineering and IT, University of Technology Sydney, Ultimo, NSW, 2007, Australia
[b] Blue Economy Cooperative Research Centre, Launceston, TAS, 7248, Australia
[c] School of Engineering, University of Southern Queensland, Toowoomba, QLD, 4350, Australia
[d] School of Engineering, Computer and Mathematical Sciences, Auckland University of Technology, Auckland, 1010, New Zealand
[e] The New Zealand King Salmon Company Limited, Nelson, 7011, New Zealand

ARTICLE INFO

Keywords:
Standalone microgrids
Renewable energy sources
Hybrid energy storage systems
Probabilistic study
Enhanced PSO

ABSTRACT

Offshore industries face significant challenges in integrating renewable energy sources (RES) to achieve a sustainable and reliable energy supply, due to the intermittency and unpredictable offshore weather conditions, which hinder the reliability of standalone microgrids. To address this issue, this study explores the integration of a hydrogen gas energy storage station within a standalone DC microgrid, evaluating its potential to enhance stability and reduce emissions in offshore maritime operations. The research investigates the effectiveness of hybrid energy storage systems (HESS) in mitigating RES intermittency, incorporating solar PV, wind, and wave energy as primary generation sources. Using an enhanced particle swarm optimisation (PSO) method, the study compares various energy storage configurations, with results indicating that a battery-supercapacitor HESS achieves the lowest levelised cost of electricity (LCOE), which is 19.63 US Cents /kWh, making it the most cost-effective solution. A probabilistic model is further developed to validate the microgrid's resilience under real-world conditions, bridging the gap between theoretical design and practical implementation. Additionally, the study assesses the feasibility of integrating wave energy, concluding that current market dynamics render it financially unviable for offshore microgrid applications. The proposed enhanced PSO algorithm demonstrates superior performance compared to commonly used heuristic optimisation methods such as Genetic Algorithm (GA), standard PSO, and Ant Colony Optimisation (ACO). This improvement is attributed to the integration of quadratic interpolation and extended local search mechanisms. Additionally, the study introduces an energy storage system (ESS) degradation algorithm that outperforms the traditional Rainflow counting method in both accuracy and computational efficiency, particularly in modelling partial charge–discharge cycles. Overall, this work provides critical insights into optimising standalone microgrids for offshore industries, alongside technical performance and economic viability.

1. Introduction

Offshore standalone DC microgrids provide a sustainable and efficient alternative to fossil fuel-powered generators for offshore platforms by integrating RES such as wind, solar, and wave energy, in conjunction with energy storage systems (ESS) with high energy density, such as batteries and hydrogen [1]. These systems help to reduce greenhouse gas emissions, lower operational costs, and minimise environmental impact while ensuring a reliable power supply. Additionally, offshore microgrids can facilitate hydrogen fuel stations for maritime transport, promoting the use of green hydrogen in fuel cell-operated vessels [2]. This transition to hydrogen-based offshore energy solutions aligns with global decarbonization efforts, supporting sustainable energy solutions for aquaculture facilities, offshore oil and gas platforms, and remote island communities.

However, the variability of RES leads to power fluctuations, placing stress on ESS, particularly batteries, and reducing their lifespan [3]. To manage these challenges, hybrid energy storage systems (HESS), combining complementary technologies such as batteries, hydrogen

* Corresponding author at: School of Electrical and Data Engineering, Faculty of Engineering and IT, University of Technology Sydney, Ultimo, NSW, 2007, Australia.
E-mail address: hasith.jayasinghe@student.uts.edu.au (H. Jayasinghe).

https://doi.org/10.1016/j.est.2025.118847
Received 27 March 2025; Received in revised form 10 September 2025; Accepted 8 October 2025
Available online 27 October 2025

Nomenclature

η_{EL}	Efficiency of PEM electrolyser
η_{FC}	Efficiency of the fuel cell stack
η_G	Combined efficiency of the generator and gear system of the wind turbine
η_{PV}	Efficiency of a solar panel
η_{WC}	Efficiency of a wave energy converter
ρ_{Air}	Density of air [kgm^{-3}]
ρ_{SW}	Density of sea water [kgm^{-3}]
A_{FC}	Area under a healthy complete cycle of the ESS
A_{Panel}	Area of solar panel [m^2]
C_D	Per unit price of diesel [USD/l]
C_{DIG}	Costs associated with the diesel generator [USD]
C_{H_2-Tank}	Capacity of Hydrogen storage tank [kg]
C_{SC}	Capacitance of SCESS [F]
$E_{BESS,Rated}$	Rated capacity of the BESS [kWh]
E_{ESS_N}	Rated capacity for Nth ESS [kWh]
E_{SC}	Energy capacity of SCESS [kWh]
EC_D	Energy content of diesel [kJ/l]
EF_D	Emission factor of diesel [t$CO_{2,eq}$/kJ]
F	Faraday constant [C/mol]
FC_{DG}	Fuel consumption rate of the diesel generator [kWh/l]
FC_{H_2}	Daily hydrogen requirement for fuel cell operation [kg]
g	Gravitational acceleration [ms^{-2}]
HFS_{H_2}	Daily hydrogen requirement for the hydrogen fuel station [kg]
hr_{max}	Maximum allowed running hours before replacement for diesel generator [hrs]
I_{DIG}	Capital cost per unit of the diesel generator [USD/kW]
I_{EL}	Per unit investment cost of electrolyser [USD/kW]
I_{ESS_N}	Per unit investment cost for Nth ESS [USD/kWh]
I_{FC}	Output current from the fuel cell stack [A]
I_{HT}	Per unit investment cost for Hydrogen storage tank [USD/kg]
I_{RG_N}	Per unit investment cost for Nth renewable energy source [USD/kW]
Irr_{max}	Maximum reported solar irradiance within a defined interval [Wm^{-2}]
k_{PV}	Temperature coefficient for solar PV [°C^{-1}]
L_{WC}	Width of wave energy converter interacting with the wave front [m]
m	inverse of the electrolyser's lifespan [year^{-1}]
m_{HT}	Capacity of Hydrogen storage tank [kg]
M_{H_2}	Molar mass of hydrogen [kgmol^{-1}]
$\dot{m}_{H_2-FS}$	Mass flow rate usage of hydrogen in the hydrogen fuel station [kgs^{-1}]
N_{Cells}	Total number of cells inside the fuel cell stack
N_{ESS}	Number of ESS elements in HESS
N_{RG_N}	Number of units for the Nth renewable energy source
OM_{DIG}	Operation and maintenance cost per unit for diesel generator [USD/kW.year]
OM_{EL}	per unit operation and maintenance cost [USD/kW]
OM_{Fixed,ESS_N}	Per unit fixed operation and maintenance cost for Nth ESS [USD/kW]
OM_{HT}	per unit operation and maintenance cost for Hydrogen storage tank [USD/kg]
OM_{RG_N}	Per unit operation and maintenance cost for Nth renewable energy source [USD/kW.year]
OM_{Var,ESS_N}	Per unit variable operation and maintenance cost for Nth ESS [USD/kWh]
P_{DIG}	Rated power of the diesel generator [kW]
P_{MG}	Rated capacity of microgrid [kW]
P_{Rated}	Rated power output of a wind turbine [kW]
P_{RG_N}	Power of a single unit for the Nth renewable energy source [kW]
PR	Performance ratio of solar PV system
R_{EL}	Per unit replacement cost of electrolyser [USD/kW]
R_{ESS_N}	Per unit replacement cost for Nth ESS [USD/kWh]
T_{Cyc}	Total cycle time of the ESS
T_{MG}	Expected lifetime of the microgrid [years]
T_{Ref}	Reference temperature of solar cell [°C]
v_{in}	Cut-in wind speed for the wind turbine [ms^{-1}]
v_{mean}	Mean wind speed [ms^{-1}]
v_{out}	Cut-off wind speed for the wind turbine [ms^{-1}]
v_{Rated}	Rated wind speed of the wind turbine [ms^{-1}]
V_{EL}	Input voltage of the electrolyser [V]
V_{FC}	Output voltage of the fuel cell stack [V]
$V_{SC-Rated}$	Rated voltage of SCESS [V]
$V_{SC}(t)$	Instantaneous voltage of SCESS [V]
x	Annual utilisation factor of the diesel generator
y	inverse of lifespan of ESS [year^{-1}]

storage, and supercapacitors (SC), are deployed to extend system life by distributing the load more effectively [4]. SCs provide a rapid response to transient power demands, thereby reducing strain on batteries, while hydrogen storage offers high energy density, enhancing overall system resilience [5]. By intelligently coordinating these storage technologies through advanced control algorithms and energy management strategies, HESS can optimise power flow, increase operational efficiency, and ensure the stability of offshore microgrids under dynamic operating conditions [6].

The integration of hydrogen production via electrolysers into offshore microgrids enables a localised, renewable-based fuel supply for fuel cell-powered vessels, enhancing sustainable energy autonomy and reducing reliance on fossil fuels. This integration also improves microgrid stability while mitigating challenges related to hydrogen storage and transportation in maritime operations [7]. The design and operation of standalone microgrids incorporating hydrogen production and storage require comprehensive planning, scheduling, and energy management due to the inherent uncertainties of renewable energy sources and the limited flexibility of electrolysers in handling input power fluctuations [8]. Advanced mathematical modelling of electrolysers and renewable energy systems, combined with robust optimisation techniques, is essential to ensure both the stability of the microgrid and the reliable operation of the electrolysers [9].

Research on the planning and design of standalone microgrids with HESS-integrated RES is rapidly expanding. In [10], the Whale Optimisation Algorithm was used to determine the optimal capacity and cost of a HESS comprising a battery and an SC, managed using a low-pass filter-based method. A GA-based energy management framework was proposed in [11] for a HESS consisting of a hydrogen storage and an SC in a standalone microgrid with a hydrogen refuelling station. In [12], a non-dominated sorting genetic algorithm II (NSGA-II) based optimisation strategy was developed for HESS sizing using a rule-based management approach. The moth flame optimisation algorithm was applied in [13] for HESS sizing, considering the uncertainty of weather parameters and load demand, with a low-pass filter used to allocate power signals between the battery and SC. In [14], a HESS comprising a battery and SC was managed using a rule-based algorithm and optimised with GA. A cuckoo optimisation-based methodology for sizing a HESS consisting of a battery and thermal energy storage, based on a rule-based energy management approach, was proposed in [15] for a standalone DC microgrid. In [16], a PSO-based approach was introduced for developing an HESS for a microgrid, employing a low-pass filter for HESS

management.

An improved ACO-based method was applied in [17] to design a HESS with a battery and hydrogen storage for cost minimisation and reliability enhancement. In [18], a HESS incorporating different battery technologies was designed for a low-voltage DC microgrid using a GA-based optimisation approach. In [19], a battery and SC-based HESS was proposed to provide inertial support for a microgrid using an enhanced PSO technique. A dynamic programming-based design for a HESS comprising a battery and SC was introduced in [20] to support vector machine application. In [21], a GA-based optimisation approach was proposed for HESS design, managed using a discrete Fourier transform method in a standalone DC microgrid. In [22], a reduced fractional gradient descent algorithm-based energy management solution was developed for designing a HESS in a standalone microgrid operating under challenging weather conditions, such as high irradiance and partial shading of solar PV. The goal was to reduce hydrogen consumption in fuel cells and utilise the produced hydrogen for ammonia production. In [23], a hybrid optimisation algorithm combining Grey Wolf Optimiser and JAYA optimisation was proposed for HESS design in a standalone DC microgrid, aiming to enhance system reliability. In [24], an energy compensation-based statistical method was used for sizing a standalone microgrid, incorporating two different battery technologies within the HESS to meet reliability and economic expectations.

The influence of varying climate conditions was effectively managed using a battery and hydrogen-based HESS in [25], where analysis conducted in HOMER software demonstrated that the HESS could efficiently handle climate variations while maintaining costs at a stable level. In [26], a generalised reduced gradient algorithm-based design strategy was proposed for a standalone DC microgrid, ensuring autonomous operation of a 100 % renewable-powered system without failures. In [27], HOMER software was used to design a standalone DC microgrid powered entirely by RES with an HESS. The results showed an unmet load of less than 0.2 %, demonstrating high system reliability. In [28], a HESS was implemented to extend the battery system's lifespan in microgrid design, resulting in a 14.8 % increase in battery lifetime. The ageing of the ESS was assessed using the rainflow cycle counting method. In [29], a standalone DC microgrid was designed using a modified fuzzy logic super-twisting algorithm, where hydrogen was utilised for fuel cell operation to support both microgrid functions and an electric vehicle charging station.

In [30], a Mixed-Integer Linear Programming (MILP) based optimisation method was employed to minimise the operation and maintenance costs of a DC microgrid, achieving full recovery of the initial investment within 6 years. In [31], an NSGA-II-based optimisation approach was utilised to design an HESS comprising Hydrogen energy

Table 1
Summary of recent significant literature on utilising HESS for standalone microgrid design.

Reference	ESS	Optimisation Strategy	HESS Management Approach	Hydrogen Production	Consideration of the uncertainty of inputs	Applicability in an offshore environment	Consideration of Degradation Effects
[10]	Battery, SC	Whale Optimisation Algorithm	Low-pass filter	×	×	×	×
[11]	Hydrogen, SC	GA	Low-pass filter	✓	×	×	×
[12]	Battery, SC	NSGA-II	Rule-based	×	×	×	×
[13]	Battery, SC	Moth flame optimisation	Low-pass filter	×	✓	×	×
[14]	Battery, SC	GA	Rule-based	×	×	×	×
[15]	Battery, Thermal ESS	Cuckoo Optimisation	Rule-based	×	✓	×	×
[16]	Battery, SC	PSO	Low-pass filter	×	×	×	×
[17]	Battery, FC	ACO	Rule-based	×	×	×	×
[18]	New Li Ion Battery, Second Life Li Ion Battery, Lead Acid Battery	GA	Rule-based	✓	×	×	×
[19]	Battery, SC	PSO	Rule-based	×	×	×	×
[20]	Battery, SC	Dynamic programming	Rule-based	×	×	×	✓
[21]	Battery, SC	GA	Discrete Fourier Transform	×	×	×	×
[22]	Battery, SC, Hydrogen	Reduced Fractional Gradient Descent Algorithm	Low Pass Filter (Primary & Secondary)	✓	✓	×	×
[23]	Battery, SC	JAYA / Grey Wolf Optimisation	Rule-based	×	×	×	✓
[24]	Two Battery technologies	Statistical	Rule-based	×	×	×	✓
[25]	Battery, Hydrogen Storage	HOMER Optimiser	Rule based	✓	×	×	×
[26]	ZnBr Battery, Pumped Hydro	Generalised Reduced Gradient Algorithm	Rule-based	×	×	×	×
[27]	Battery, SC	HOMER Optimiser	Rule-based	×	×	×	×
[28]	Battery, SC	Rainflow Counting Algorithm	Low Pass Filter	×	×	×	✓
[29]	Battery, Hydrogen Storage	Fuzzy Logic-based Modified Super Twisting Algorithm	Low Pass Filter	✓	×	✓	×
[30]	Battery, Hydrogen Storage	MILP	Rule-based	✓	×	×	×
[31]	Battery, Hydrogen Storage	NSGA-II	CEEMDAN	✓	×	×	×
[32]	Battery, Hydrogen Storage	MILP / MIQP	Low-pass Filter	✓	×	×	×
This study	Battery, SC, Hydrogen Storage	Modified PSO	Low-pass filter	✓	✓	✓	✓

storage and BESS in a standalone DC microgrid. In this study, Complete Ensemble Empirical Mode Decomposition with Adaptive Noise (CEEMDAN) was developed to decompose power fluctuations into high- and low-frequency components. In [32], a design methodology combining MILP and Mixed Integer Quadratic Programming (MIQP) was proposed for a standalone DC microgrid with Hydrogen and Battery HESS, resulting in reduced total operating costs and pollutant emission costs. Table 1 summarises the key gaps and unmet factors identified in the research on HESS for standalone DC microgrids.

Most of the literature reviewed focuses on applying novel optimisation algorithms to minimise costs and reduce simulation time. Among these, PSO has been the most widely utilised due to its ability to achieve fast convergence in large solution spaces [33]. However, heuristic algorithms, including PSO, are prone to trapping in local minima, and techniques such as local search, partial integration of mathematical optimisation, and parallel computing, which could mitigate this issue, are rarely discussed in the literature. Additionally, limited studies assess the techno-economic feasibility of offshore standalone microgrids utilising specific RES, such as wave energy, in combination with offshore hydrogen refuelling stations for vessels. The cost-effectiveness of hydrogen energy storage compared to batteries in hydrogen-based microgrids, particularly where investments in hydrogen production have already been made, has not been thoroughly analysed in the current literature, especially considering the high costs associated with fuel cells. Offshore microgrids also face significant uncertainty in key input parameters such as solar irradiation and wind speed, yet only a limited number of studies employ probabilistic analysis to account for this variability and improve design accuracy [34]. Furthermore, the degradation of ESS due to factors such as cycle life and temperature is often overlooked, despite its impact on system lifespan and maintenance costs. Standard methods, such as the Rainflow counting algorithm, cannot accurately capture the partial charge-discharge cycles of ESS, making them unsuitable for standalone DC microgrids, where frequent partial cycling occurs throughout the day [35]. Addressing these gaps is essential for the advancement of offshore hydrogen-based microgrids and the development of more reliable, efficient and cost-effective energy storage solutions.

This study addresses the critical design challenge of determining an optimal sizing strategy for RES and ESS in a standalone hydrogen-based microgrid. The primary objective is to balance the total net present value of costs while leveraging technological advances through ESS hybridisation, integrating diverse RES in offshore environments, and producing green hydrogen at minimal cost for fuel stations. The inclusion of multiple RES and ESS technologies, each with unique characteristics, increases the complexity of the design [36]. To address this, an intelligent energy management model is integrated into the microgrid design to optimally allocate ESS technologies to meet demand, identify which RES should be prioritised to minimise lifecycle costs, and determine the most cost-effective timeframes for hydrogen production. To further enhance the design methodology, this study introduces a novel optimisation framework to address key research gaps in standalone microgrid development with on-site hydrogen production for offshore applications, with the following novel features.

- An enhanced PSO algorithm integrating Quadratic Interpolation with an extended local search is presented for determining optimal design parameters of a standalone DC microgrid. The integration of quadratic interpolation with extended local search effectively mitigates the issue of local minima commonly encountered in standard PSO.
- A comprehensive framework for ESS degradation quantification is developed, enabling the integration of future advancement and replacement costs into the optimisation cost function. This framework accurately captures partial charge-discharge cycles, improving the reliability of lifecycle cost estimation.
- A mathematical model of wave energy is incorporated into the cost function to evaluate the techno-economic feasibility of wave energy in the design of offshore standalone DC microgrids.
- The proposed optimisation framework for designing a standalone DC microgrid with a hydrogen fuel station is evaluated under three scenarios of ESS: (i) battery only, (ii) battery + SC HESS, and (iii) hydrogen + SC HESS, to determine the optimal energy storage combination.
- A scenario-based probabilistic analysis is conducted to assess the impact of uncertainty of input variables, such as variability in RES, on the design and performance of the standalone DC microgrid.

The sections of the manuscript are organised as follows. Section 2 describes the design of each component within the offshore standalone DC microgrid, including ESS cycle life considerations and the distribution of power signals among multiple ESS technologies. Section 3 defines the objectives, constraints, and methodologies employed for optimal microgrid design. Section 4 presents a case study demonstrating the application of the proposed methodologies. Section 5 presents the simulation results, including comparisons across multiple scenarios, and provides design recommendations. Section 6 explains the superiority of the proposed enhanced PSO methodology compared to conventional heuristic optimisation techniques, as well as the effectiveness of the proposed ESS degradation quantification framework. Section 7 outlines future research directions emerging from this study, followed by a conclusion that provides a concise summary of the key findings.

2. Design of standalone hydrogen-based DC microgrid

This study proposes a design for a hydrogen-based standalone DC microgrid for offshore applications, featuring a DC bus architecture that interconnects generation sources, loads, and ESS components. The microgrid integrates solar PV, wind, and wave energy as RES, with a diesel generator serving as a backup, as illustrated in Fig. 1. The load profile includes offshore site demands and a hydrogen fuelling station. Three ESS configurations are analysed to determine the optimal solution for this application. In the first two scenarios, (1) battery-only, and (2) battery + SC HESS, the hydrogen fuelling station operates solely as a load, with an electrolyser producing hydrogen exclusively for refuelling purposes. In the third scenario, where a hydrogen storage + SC HESS is proposed, the electrolyser generates hydrogen for both the fuelling station and a fuel cell, which supplies power to the microgrid. In this configuration, the hydrogen system, including the electrolyser, hydrogen storage tank, and fuel cell, functions as both a load and an ESS. The study aims to identify the most cost-effective ESS configuration by evaluating lifecycle costs for offshore applications.

2.1. Model of solar PV system

Solar PV is a strong candidate for microgrid design due to its ease of implementation, low manufacturing costs, and zero emissions after installation [37]. The maximum power output (P_{PV}), which is influenced by site-specific solar irradiation (Irr) and cell temperature (T_C), is calculated using Eq. (1) [38].

$$P_{PV} = \eta_{PV}.(PR).(Irr).A_{Panel}.\left(1 - k_{PV}.\left(T_C - T_{Ref}\right)\right) \quad (1)$$

Solar irradiance can be modelled using a Beta distribution for probabilistic analysis and is estimated using Eqs. (2), (3) and (4) below [39]. Here α, β are the shape parameters of the Beta distribution, and μ, and σ are the mean and standard deviation (SD) of a probabilistic distribution.

$$f\,(Irr) = \frac{\Gamma(\alpha+\beta)}{\Gamma(\alpha).\Gamma(\beta)}.\left(\frac{Irr}{Irr_{max}}\right)^{\alpha-1}.\left(1-\frac{Irr}{Irr_{max}}\right)^{\beta-1} \quad (2)$$

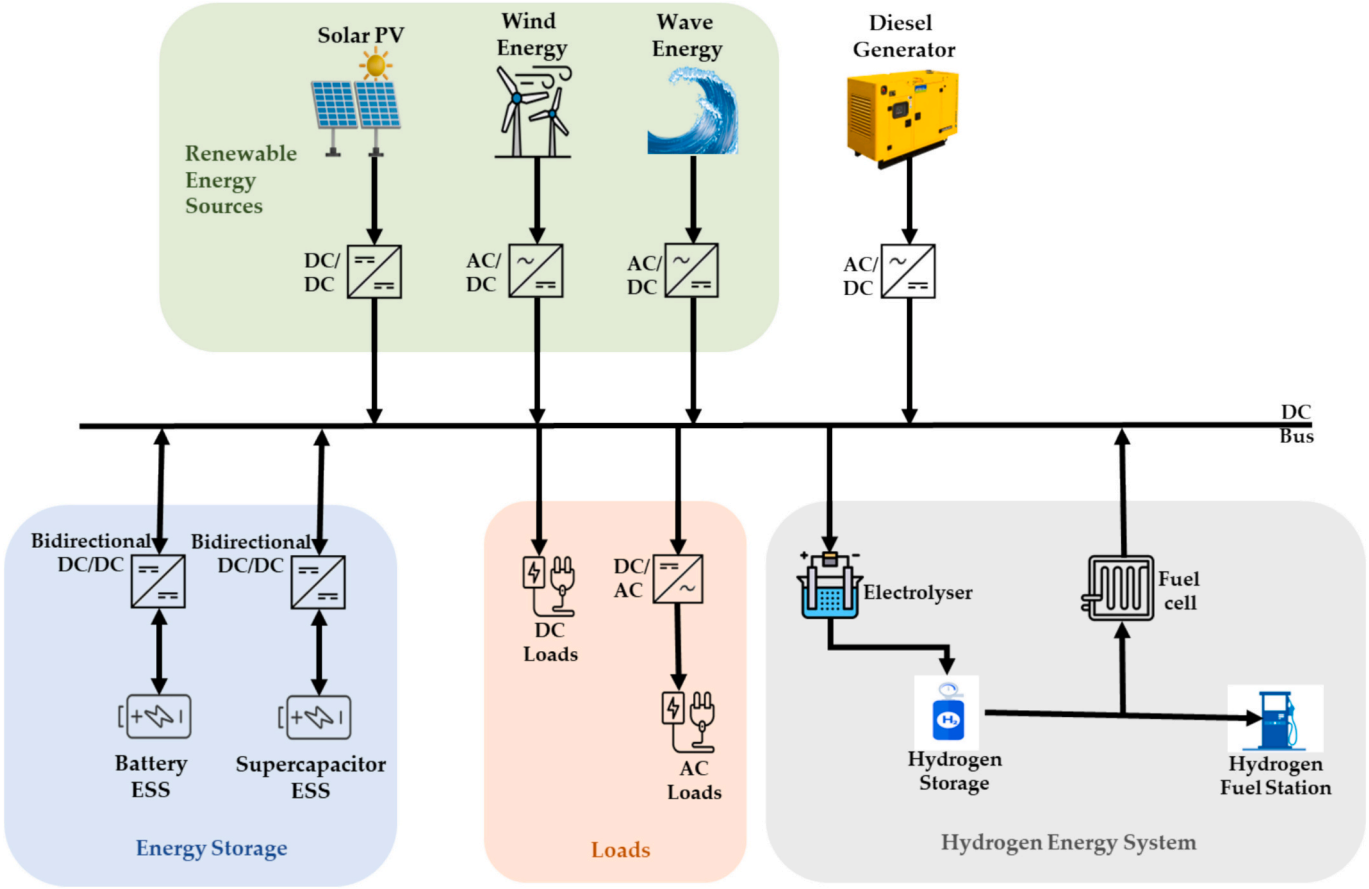

Fig. 1. Architecture of proposed standalone DC microgrid.

$$\alpha = \mu.\left(\frac{\mu(1-\mu)}{\sigma^2} - 1\right) \tag{3}$$

$$\beta = (1-\mu).\left(\frac{\mu(1-\mu)}{\sigma^2} - 1\right) \tag{4}$$

2.2. Wind turbine system

Wind turbines convert the kinetic energy of wind into electricity and can be installed either onshore or offshore [40]. Power generation depends on wind speed (v_{Wind}) and rotor swept area (A_{Swept}), with the power output (P_{WT}) calculated using Eq. (5) [41].

$$P_{WT} = \begin{cases} \frac{1}{2}.\eta_G.C_P.A_{Swept}.\rho_{Air}.v_{Wind}^3; \text{if } v_{in} \le v_{Wind} \le v_{Rated} \\ P_{Rated}; \text{if } v_{Rated} \le v_{Wind} \le v_{out} \\ 0; \text{otherwise} \end{cases} \tag{5}$$

Wind speed is a stochastic variable that can be modelled using a Weibull distribution for probabilistic studies, where c and k are the scale factor and shape factor of the probability density function (PDF), and is estimated using Eqs. (6), (7), and (8) provided below [42].

$$f(v_{Wind}) = \frac{k.v_{wind}^{k-1}}{c^k}.e^{-\left(\frac{v_{Wind}}{c}\right)^k} \tag{6}$$

$$k = \left(\frac{\sigma_v}{v_{mean}}\right)^{-1.086} \tag{7}$$

$$c = \frac{v_{mean}}{\Gamma\left(1+\frac{1}{k}\right)} \tag{8}$$

2.3. Wave energy system

Wave energy, derived from ocean waves, is a promising RES due to its higher energy density and greater consistency compared to other renewables. It harnesses the kinetic and potential energy of wind-driven waves to generate electricity. Advancements in wave energy converters (WECs) aim to enhance efficiency while minimising environmental impact [43]. Ocean waves are primarily driven by wind, and since wind energy prediction methods are well-established, wave data can be forecasted using the correlation between wind speed and wave energy parameters [44]. The power density of ocean waves (P_{Wave}) is typically calculated based on wavefront width, as shown in Eq. (9) [45].

$$P_{Wave} = \frac{\rho_{SW}.g^2}{64\pi}.h_W{}^2.T_W \tag{9}$$

Wave height (h_W) and wave period (T_W) can be estimated from wind speed data using a wave power prediction model, as expressed in Eqs. (10) and (11), which incorporate the parameters a, b, c, and d [44]. The output power of a WEC (P_{WC}) is then calculated using Eq. (12), subject to the operating condition $h_{CI} \le h_W \le h_{CO}$, where h_{CI} and h_{CO} denote the cut-in and cut-off wave heights, respectively. When $h_W < h_{CI}$, the device motion is insufficient to drive the power take-off (PTO) effectively. In this case, the harvested energy cannot compensate for mechanical and electrical losses, resulting in negligible net output. Conversely, when $h_W > h_{CO}$, the forces exerted on the device and its PTO system become excessive. Operating under such extreme conditions risks structural

damage, fatigue, or PTO failure; therefore, the WEC incorporates protective measures by shutting down [46].

$$h_W = a.v_{wind}^{b} \tag{10}$$

$$T_W = c.v_{wind}^{d} \tag{11}$$

$$P_{WC} = \begin{cases} 0, h_W < h_{CI} \\ \eta_{WC}.P_{Wave}.L_{WC}, h_{CI} \le h_W \le h_{CO} \\ 0, h_W > h_{CO} \end{cases} \tag{12}$$

2.4. Diesel generator

Due to the intermittent nature of RES, a backup power source —typically a diesel generator —is essential in standalone DC microgrids. Diesel generators are easy to install, have a low initial cost, and offer reliable long-term operation [47]. However, they have notable drawbacks, including high operational costs, frequent maintenance requirements, and significant carbon emissions. Diesel generators are typically sized to meet peak demand, but this approach results in inefficient low-load operation during periods of reduced demand, thereby increasing operational and maintenance costs [48]. To mitigate these issues, it is recommended to operate the diesel generator at a constant load with an optimal loading percentage [49]. In [50], it is suggested that the optimal loading level is approximately 75 % of full capacity. Therefore, this study assumes the diesel generator operates at 75 % of its rated full load.

2.5. Battery energy storage system (BESS)

BESS have gained popularity due to their high efficiency, low manufacturing costs, and minimal environmental impact. Various battery technologies, including lithium-ion, lead-acid, graphene, and sodium-ion, are available for microgrid applications [51]. Lithium-ion batteries stand out for their high efficiency, flexible discharge profiles, and long operational lifespan, making them the preferred choice. With a significant reduction in manufacturing costs, lithium-ion technology has become the leading option for BESS in microgrid systems [52]. In this study, lithium-ion batteries are selected as the ESS for the standalone DC microgrid design. The State of charge (SOC) of a BESS is calculated as the ratio of the instantaneous energy capacity ($E_{BESS}(t)$) to the rated energy capacity ($E_{BESS,Rated}$), as shown in Eq. (13) below.

$$SOC_{BESS}(t) = \frac{E_{BESS}(t)}{E_{BESS,Rated}} \tag{13}$$

2.6. Supercapacitor Energy Storage System (SCESS)

SCESS offer high power density, rapid charge-discharge capability, and a long operational lifespan, making them ideal for stabilising microgrids during power fluctuations. SCESS complements other storage technologies by providing short-term energy buffering, thereby improving overall efficiency and resilience [53]. This study examines the effectiveness of SCESS in mitigating high power fluctuations in conjunction with BESS and hydrogen energy storage. To manage power fluctuations effectively, SCESS must be capable of quickly absorbing or releasing energy, which requires it to remain readily available during microgrid operation. A focused SOC range is proposed, with $SOC_{SC\text{-}FL}$ near 50 % and $SOC_{SC\text{-}FH}$ near the maximum allowed SOC, as illustrated in Fig. 2 [14]. SCESS should maintain its SOC within this range and promptly return to it if deviations occur. The SOC and energy requirements of SCESS are calculated using Eqs. (14) and (15).

$$SOC_{SC}(t) = \frac{V_{SC}(t)}{V_{SC-Rated}} \tag{14}$$

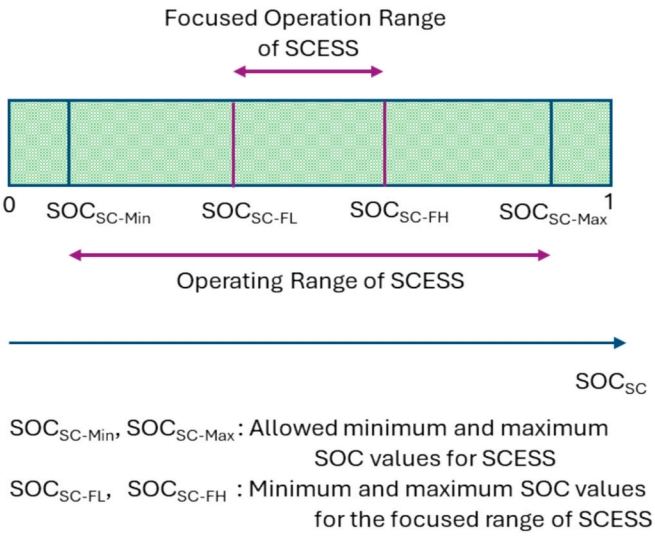

Fig. 2. Focused operation range vs. allowed operation range for SCESS.

$$E_{SC} = \frac{1}{2}.C_{SC}.V_{SC-Rated}.\left(SOC_{SC-Max}^{2} - SOC_{SC-Min}^{2}\right) \tag{15}$$

2.7. Fuel cell

Hydrogen fuel cells provide a clean, efficient, and scalable power source by converting hydrogen into electricity with minimal emissions. Their integration into microgrids enables continuous power generation, thereby reducing reliance on intermittent RES. With high energy density and operational adaptability, fuel cells enhance energy security, reduce environmental impact, and improve system flexibility [54]. Eq. (16) represents the total power output of the fuel cell stack (P_{FC}), while the hydrogen mass flow rate ($\dot{m}_{H_2-FC}$) is calculated using Eq. (17).

$$P_{FC} = V_{FC}.I_{FC} \tag{16}$$

$$\dot{m}_{H_2-FC} = \frac{P_{FC}.N_{Cells}.M_{H_2}}{2.F.\eta_{FC}.V_{FC}} \tag{17}$$

2.8. Proton Exchange Membrane (PEM) electrolyser

PEM electrolysers are ideal for offshore hydrogen production due to their high efficiency, rapid response times, and compact design. Their ability to operate at high pressures makes them well-suited for integration with RES, supporting decarbonization of maritime industries by reducing dependence on fossil fuels. Also, their modularity and scalability enable flexible energy solutions for offshore operations [55]. In this study, a PEM electrolyser is utilised to produce hydrogen for a fuelling station within the microgrid, with the generated hydrogen also used to power fuel cells as part of the ESS. The PEM electrolyser draws power from the DC microgrid to split water into hydrogen and oxygen. The hydrogen production rate ($\dot{m}_{H_2-EL}$) is calculated using Eq. (18).

$$\dot{m}_{H_2-L} = \frac{\eta_{EL}.P_{EL}.M_{H_2}}{2.F.V_{EL}} \tag{18}$$

The system efficiency of the electrolyser depends on multiple factors. Eq. (19) below calculates the system efficiency by multiplying Faraday's efficiency (η_{EL}^{F}), hydrogen production efficiency (η_{EL}^{H}), and compression efficiency (η_{EL}^{C}). η_{EL}^{F} accounts for the loss due to the permeation of Hydrogen, which is the unintended move of hydrogen gas through the PEM from the cathode to the anode side, as presented in Eq. (20) below.

η_{EL}^{H} is calculated in Eq. (21) below, which relates to the temperature and pressure differences in the electrochemical reaction stage.

$$\eta_{\mathrm{EL}} = \eta_{EL}^{F}.\eta_{EL}^{H}.\eta_{EL}^{C} \tag{19}$$

$$\eta_{EL}^{F} = \left[1 - \frac{2.V_{EL}\left(F.P_{H_2}^{T}.\frac{P_{EL}^{H_2}+P_{EL}^{O_2}}{d_{el}.\delta_{el}} + \frac{a_x.P_{EL}}{d.\delta}\right)}{P_{EL}}\right] \tag{20}$$

$$\eta_{EL}^{H} = \frac{125}{1.229 + \left|1.48 + \frac{\Delta H_{Vap}.P_{H_2O}}{2F}\left(\frac{1}{P_{EL}^{H_2}} + \frac{1}{P_{EL}^{O_2}}\right) - U_{Cell}\right| + \frac{R.T_{Cell}}{2F}\ln\left(\frac{P_{EL}^{H_2}.P_{EL}^{O_2}}{(P_o)^{1.5}}\right) + \frac{P_{EL}(\sigma_{el}.r_0+d_{el}.\delta_{el})}{\sigma_{el}.V_{EL}} - \frac{0.9(T_{Cell}-298)}{1000}} \tag{21}$$

2.9. Hydrogen storage tank

Hydrogen produced by the electrolyser is stored in gaseous form in high-pressure tanks, typically operating within a range from 350 to 700 bar, offering high energy density while ensuring safe storage. Tank materials, such as carbon fibre composites or high-strength steel, are selected to ensure structural integrity under varying environmental and operational conditions [56]. The quantity of hydrogen stored at the time t_2 $\left(m_{H_2-Tank}(t_2)\right)$ is calculated using the mass balance equation, as shown in Eq. (22).

$$m_{H_2-Tank}(t_2) = m_{H_2-Tank}(t_1) + (t_2 - t_1).\left[\dot{m}_{H_2-EL}(t_2) - \dot{m}_{H_2-FC}(t_2) - \dot{m}_{H_2-FS}(t_2)\right] \tag{22}$$

2.10. Power converters

Power converters play a crucial role in facilitating power conversion and integration within standalone microgrids. The solar PV system is interfaced with the DC bus via a unidirectional DC/DC converter equipped with maximum power point tracking (MPPT) functionality to optimise energy extraction. Other renewable energy sources, which typically produce AC power, are converted to DC using unidirectional AC/DC converters, also featuring MPPT capabilities [57]. Bidirectional DC/DC converters are employed to interface both the BESS and the SCESS with the DC bus, enabling controlled charging and discharging operations [58]. When the fuel cell is integrated into the microgrid configuration, it is connected to the DC bus via an additional DC/DC converter. To accommodate both DC and AC loads, appropriate conversion technologies are utilised: DC/DC converters are used for DC loads, while DC/AC converters are employed to supply AC loads from the DC bus [59].

In this study, the efficiency of these power electronic controllers is modelled and incorporated into the objective function of the optimisation problem. To represent controller efficiency, the European weighted efficiency model η_{EUR}, is employed [60]. This model is expressed by Eq. (23), where $\eta_{X(5\%,10\%,\ldots,100\%)}$ denotes the efficiency at a specific power output level, given as a percentage of the converter's rated power output.

$$\eta_{\mathrm{EUR}} = 0.03\eta_{5\%} + 0.06\eta_{10\%} + 0.13\eta_{20\%} + 0.10\eta_{30\%} + 0.48\eta_{50\%} + 0.20\eta_{100\%} \tag{23}$$

3. Methodology

This study presents the design of a standalone DC microgrid powered by RES to support an offshore facility equipped with a hydrogen fuel station. The proposed strategy focuses on minimising the microgrid's lifecycle cost through the implementation of a HESS, accounting for investment, replacement, operation, maintenance, and carbon tax costs. The following subsections provide a detailed description of the proposed optimisation strategy, which incorporates a probabilistic approach to address uncertainties in input parameters, such as weather conditions. This method enables the identification of best- and worst-case scenarios, which can be utilised in the design process, depending on the criticality of the power supply requirements for the connected loads.

3.1. Objective function

The objective function for the optimisation problem is defined in Eq. (24), where C_{LC} is the lifecycle cost of the standalone DC microgrid. To account for future expenses, the net present value (NPV) method is employed to aggregate all cost components, into a unified framework for analysis.

$$C_{LC} = C_{RG} + C_{DIG} + C_{ESS} + C_{HFS} \tag{24}$$

In this study, solar PV, wind, and wave energy are selected as RES. The lifecycle cost of RES (C_{RG}) is represented in Eq. (25) below.

$$C_{RG} = \sum_{N=1}^{3}\left[N_{RG_N}.P_{RG_N}.\left(I_{RG_N} + \sum_{i=1}^{T_{MG}}\frac{OM_{RG_N}}{(1+r)^{T_{MG}-(i+1)}}\right)\right] \tag{25}$$

The lifetime costs of the diesel generator within the microgrid are represented by Eq. (26). To account for carbon emissions, a carbon tax (CT) is incorporated into the cost calculation [61].

$$C_{DIG} = P_{DIG}.\left(\sum_{i=1}^{T_{MG}}\frac{OM_{DIG} + x.FC_{DIG}.C_D.hr_{max}}{(1+r)^{T_{MG}-(i+1)}} + \sum_{i=0}^{x.T_{MG}}\frac{I_{DIG}}{(1+r)^{T_{MG}-\frac{i}{x}}}\right) + \sum_{i=1}^{T_{MG}}\frac{FC_{DIG}.x.hr_{max}.EC_D.EF_D.CT}{1000.(1+r)^{T_{MG}-(i+1)}} \tag{26}$$

This study investigates the effectiveness of hybridising ESS, including BESS, SCESS and fuel cells, alongside hydrogen energy storage. The costs associated with ESS (C_{ESS}) are represented in Eq. (27). For fuel cells, Eq. (27) should replace $(SOC_{Max} - SOC_{Min})$ term with a constant (i.e., 1), since fuel cells do not undergo a conventional charging

process. Instead, hydrogen production and storage required for fuel cell operation are managed by the electrolyser and hydrogen storage tank

$$C_{H_2-Tank} \geq m_{H_2-Tank}(t-1) + m_{H_2-EL}(t) - (m_{H_2-HFS}(t) + m_{H_2-FC}(t)) \quad (32)$$

$$C_{ESS} = \sum_{N=1}^{N_{ESS}} \left[E_{ESS_N} \cdot \left(I_{ESS_N} + \sum_{i=1}^{T_{MG}} \frac{OM_{Var,ESS_N}}{(1+r)^{T_{MG}-(i+1)}} + \sum_{i=0}^{y.T_{MG}} \frac{R_{ESS_N}}{(SOC_{Max} - SOC_{Min}).(1+r)^{T_{MG}-\frac{i}{y}}} \right) + P_{MG} \cdot \sum_{i=1}^{T_{MG}} \frac{OM_{Fixed,ESS_N}}{(1+r)^{T_{MG}-(i+1)}} \right] \quad (27)$$

The costs associated with a hydrogen fuel station (C_{HFL}) are divided into two main components: the electrolyser and the hydrogen storage tank, as represented by Eq. (28).

$$C_{HFL} = E_{EL} \cdot \left(I_{EL} + \sum_{i=1}^{T_{MG}} \frac{OM_{EL}}{(1+r)^{T_{MG}-(i+1)}} + \sum_{i=0}^{m.T_{MG}} \frac{R_{EL}}{(1+r)^{T_{MG}-\frac{i}{m}}} \right) + m_{HT} \cdot \left(I_{HT} + \sum_{i=1}^{T_{MG}} \frac{OM_{HT}}{(1+r)^{T_{MG}-(i+1.)}} \right) \quad (28)$$

3.2. Constraints

The optimisation strategy proposed in this study incorporates multiple constraints to satisfy the requirements of the optimisation problem. Constraint (29) ensures power balance, which is critical for the reliability of the microgrid. Its primary objective is to maintain the total microgrid demand, comprising both the load demand and the electrolyser unit's load, below the combined output from energy sources and the power discharged from the ESS. When the ESS is charging, the sign of $P_{ESS}(t)$ becomes negative, thereby contributing to the demand side of the inequality. Constraint (30) regulates hydrogen production to meet the requirements of both the hydrogen refuelling station and fuel cell operations. The total daily hydrogen demand from these two components, considered only in the hydrogen + SC HESS configuration, must not exceed the daily hydrogen production from the electrolyser unit.

The SOC constraint, represented by constraint (31), applies exclusively to BESS and SCESS. The proposed maximum and minimum SOC limits for charging and discharging are intended to mitigate overheating, which can adversely affect the lifespan of the ESS [33]. For hydrogen energy storage, constraint (32) ensures that the hydrogen tank capacity consistently exceeds the required hydrogen demand. At each timestep, the tank capacity is updated by adding the hydrogen produced during that interval to the existing hydrogen volume from the previous timestep, and subtracting the hydrogen utilised by the refuelling station and fuel cell if present.

To minimise energy losses due to RES curtailment, constraint (33) imposes a limit on the maximum allowable curtailment. In this study, the permitted curtailment is restricted to less than 5 % of the daily renewable energy generation [62]. Finally, constraint (34) ensures that the LCOE remains below a specified threshold, thereby maintaining the economic viability of the microgrid. The maximum allowable LCOE is set at 25 % above that of a standalone diesel generator-based power system [63]. This additional margin accounts for the increased cost associated with integrating hydrogen and SC-based HESS into the microgrid.

$$P_D(t) + P_{EL}(t) \leq P_{RG}(t) + P_{DIG}(t) + P_{ESS}(t) \quad (29)$$

$$m_{H_2-EL} \geq HFS_{H_2} + FC_{H_2} \quad (30)$$

$$SOC_{Min} \leq SOC_{ESS}(t) \leq SOC_{Max} \quad (31)$$

$$E_{Waste} \leq E_{Waste-Max} \quad (33)$$

$$LCOE \leq LCOE_{Max} \quad (34)$$

3.3. Energy management criterion for HESS

This study introduces a novel energy management criterion for standalone DC microgrids, considering the SOC of different components in HESS, as presented in the following set of equations. Eq. (35) defines the instantaneous power ($P_{ESS}(t)$) managed by the ESS as the difference between total demand ($P_{TD}(t)$) and renewable generation ($P_{RG}(t)$), while Eq. (36) calculates total power demand, which the generation must meet from RES, and must satisfy both the instantaneous site load requirements ($P_D(t)$) and electrolyser power demand ($P_{EL}(t)$).

$$P_{ESS}(t) = P_{TD}(t) - P_{RG}(t) \quad (35)$$

$$P_{TD}(t) = \begin{cases} P_D(t) + P_{EL}(t), if\ P_{RG}(t) \geq P_D(t) + P_{EL}(t) \\ P_D(t), otherwise \end{cases} \quad (36)$$

A second-order passive low-pass energy filter is employed to distribute the power demand between ESS, offering the advantage of reduced computational complexity [64]. The high-energy-density ESS manages the low-frequency component of the demand signal. In contrast, the high-frequency component, obtained by subtracting the low-frequency signal from the original, is handled by the high-power-capacity ESS. The transfer function of the filter ($f(s)$) is defined in Eq. (37), where ω_n represents the cut-off frequency, and Q denotes the quality factor, which characterises the damping behaviour of the filter. To determine the optimal value for ω_n, a discrete Fourier transform-based model is used as given in Eqs. (38) to (40). Discrete Fourier transform of $P_{ESS}(t)$ is found using Eq. (38) below, where $P_{ESS}(n)$ is the discrete-time signal of $P_{ESS}(t)$. Power Spectral Density (PSD), which describes how the signal's power is distributed across frequencies, is calculated using Eq. (39) below, where $S_P(\omega_k)$ is the PSD for a certain ω_k frequency. Using the PSD values for different frequencies, the percentage of frequencies to be handled by the low-power-density ESS unit in HESS is calculated using Eq. (40). The optimal value for this percentage is determined by solving the microgrid optimisation problem, which minimises the total lifecycle cost.

$$f(s) = \frac{\omega_n^2}{s^2 + \left(\frac{\omega_n}{Q}\right)s + \omega_n^2} \quad (37)$$

$$P_{ESS}[k] = \sum_{n=0}^{N-1} P_{ESS}(n).e^{-j\frac{2\pi}{N}kn}, \text{where } k = \frac{NT_S\omega_k}{2\pi} \quad (38)$$

$$S_P(\omega_k) = \frac{1}{N}|P_{ESS}[k]|^2 \quad (39)$$

$$x_n = \frac{\int_0^{\omega_n} S_P(\omega_k)}{\int_0^{\infty} S_P(\omega_k)} \quad (40)$$

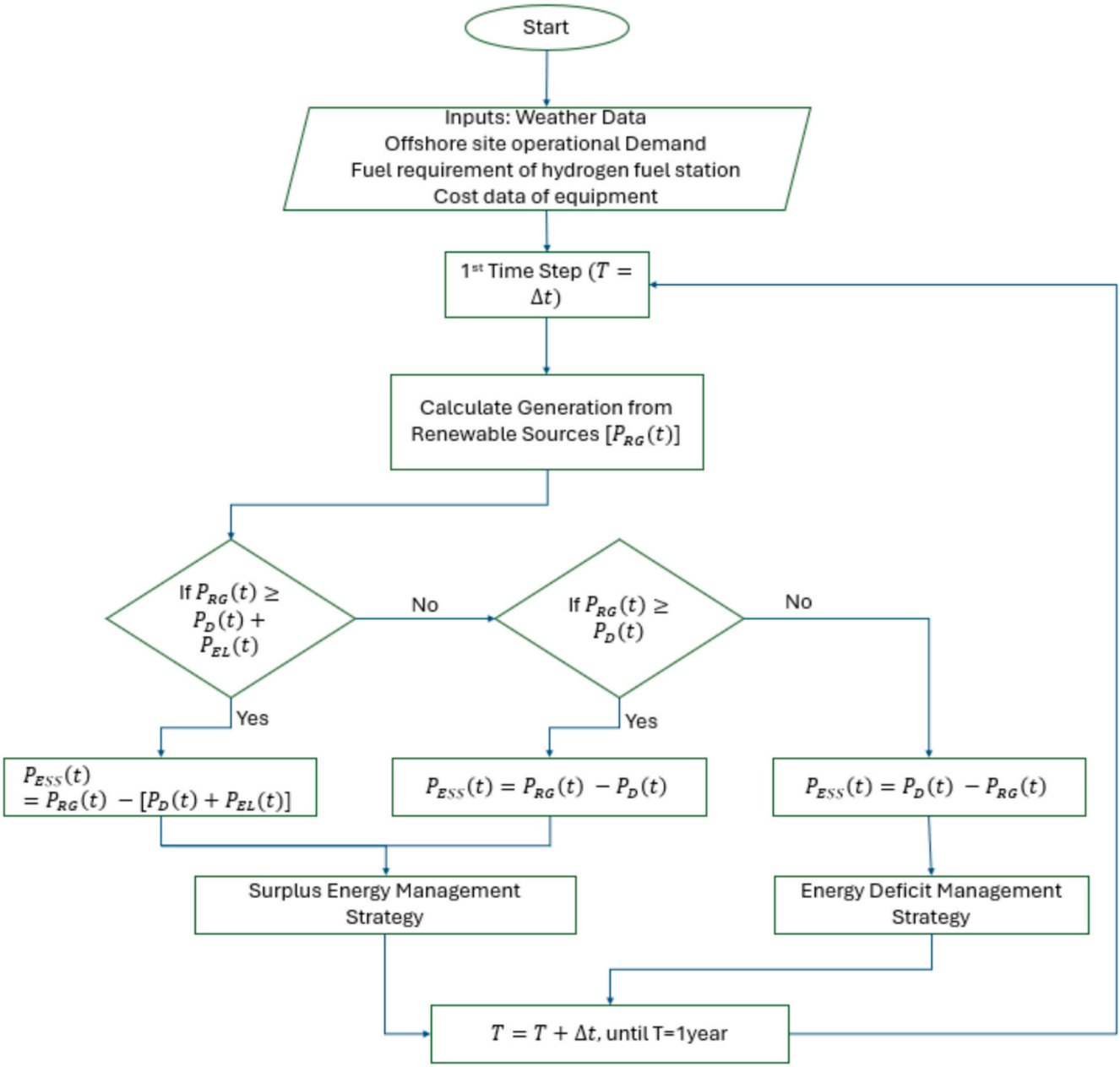

Fig. 3. Proposed energy management algorithm for the standalone DC microgrid.

In this study, RES and demand data were collected at discrete time intervals. To apply the continuous-time transfer function, it was converted to the discrete-time domain (z-domain) using Tustin's method, with the resulting transfer function shown in Eq. (41) [65]. Converting the z-domain transfer function to the time domain enables the extraction of the low-frequency component of the demand signal ($P_{LF-ESS}(t)$), which is then allocated to the appropriate ESS, which is represented in Eqs. (42) to (44), where b_0, b_1, b_2, a_1, and a_2 are constants.

$$f(z) = \frac{\omega_n^2}{\left(\frac{2}{T}\cdot\frac{1-\frac{1}{z}}{1+\frac{1}{z}}\right)^2 + \left(\frac{\omega_n}{Q}\right)\left(\frac{2}{T}\cdot\frac{1-\frac{1}{z}}{1+\frac{1}{z}}\right) + \omega_n^2} \tag{41}$$

$$P_{LF-ESS}(t) = b_0.P_{ESS}(t) + b_1.P_{ESS}(t-T) + b_2.P_{ESS}(t-2T) - a_1.P_{LF-ESS}(t-T) - a_2.P_{LF-ESS}(t-2T) \tag{42}$$

$$b_0 = \frac{b_1}{2} = b_2 = {\omega_n}^2.T^2 \tag{43}$$

$$\frac{a_1}{z} + \frac{a_2}{z^2} = \frac{4(z^2-2z+1) + 2\omega_n QT(z^2-1) + \omega_n^2 T^2(z^2+2z+1)}{T^2(z^2+2z+1)} \tag{44}$$

The high-frequency component of the power signal ($P_{HF-ESS}(t)$) is obtained by subtracting the low-frequency component from the original power signal supplied to the ESS, as described in Eq. (45). The overall energy management criterion for the HESS and microgrid is illustrated in Fig. 3. Based on the generation surplus or deficit at a given time, this criterion selects either the surplus energy management strategy or the deficit energy management strategy, which are depicted in Figs. 4 and 5, respectively.

$$P_{HF-ESS}(t) = P_{ESS}(t) - P_{LF-ESS}(t) \tag{45}$$

In the case of a fuel cell, both ramp-up and ramp-down rates exist when transitioning between power levels or during startup. During these

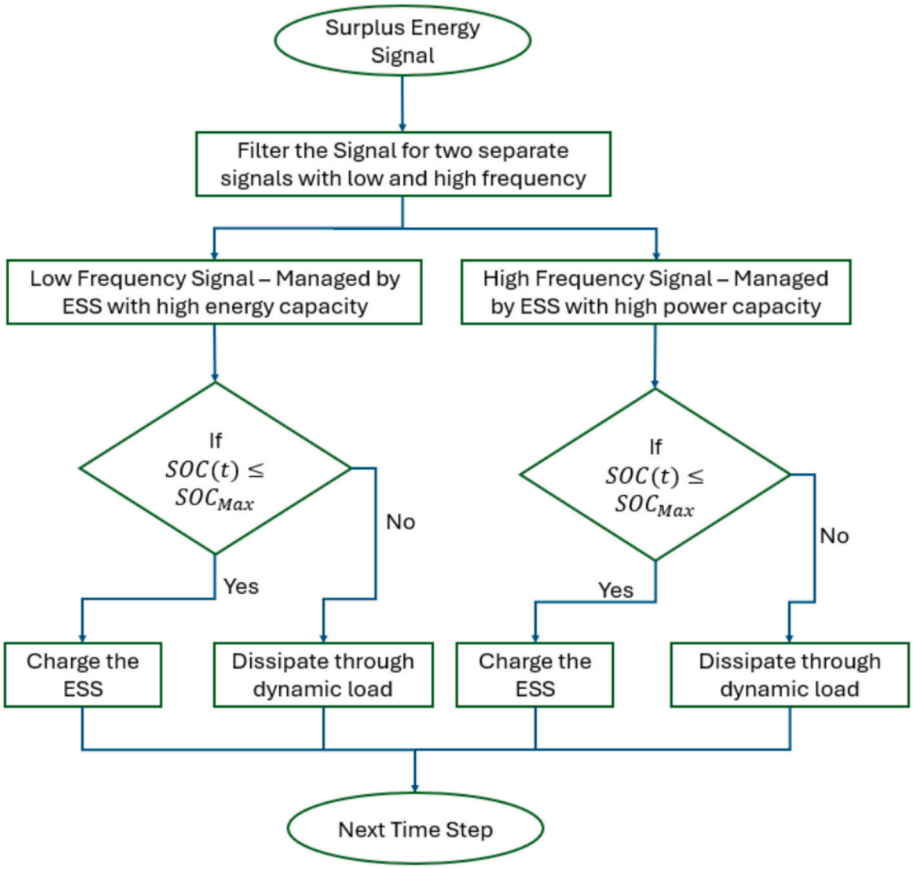

Fig. 4. Surplus energy management strategy.

ramping periods, the SCESS supports the fuel cell by compensating for the portion of power that the fuel cell cannot supply or absorb [66]. The following Eqs. (46) and (47), describe the power management strategy during the ramp-up and ramp-down processes, where R_{FC} denotes the fuel cell ramp rate, and $P_{FC}(t')$ and $P_{SC}(t')$ represent the power contributions from the fuel cell and SCESS, respectively, during these periods.

$$P_{FC}(t') = \text{Min}\left[P_{LF-ESS}(t+T), P_{LF-ESS}(t) + R_{FC}.(t'-t)\right] \quad (46)$$

$$P_{SC}(t') = P_{ESS}(t+T) - P_{FC}(t') \quad (47)$$

3.4. Cycle counting algorithm for ESS

When designing an ESS, it is essential to account for its degradation over time, which is measured by its cycle life, to ensure optimal technical and economic performance. Cycle life is affected by various factors, including temperature, charge/discharge profiles, and depth of discharge. It is typically evaluated by counting the number of cycles until the manufacturer's specified limit is reached, at which point the ESS must be replaced [67]. Drawing inspiration from the Rainflow cycle counting method used in material fatigue analysis, the proposed cycle counting algorithm for ESS monitors the area under the SOC curve at each time step to quantify complete cycles. Eq. (48) calculates the triangular areas illustrated in Fig. 6, while Eq. (49) determines the total cycle duration of the ESS. The flowchart for the algorithm is shown in Fig. 7.

$$A_n = \frac{\Delta T.|SOC_n - SOC_{n-1}|}{2} \quad (48)$$

$$T_{Cyc} = \frac{\sum_{n=1}^{T_{MG}} A_n}{A_{FC}} \quad (49)$$

The ageing of ESS exhibits a nonlinear relationship with factors such as temperature, pressure, and depth of discharge (DOD), rather than solely depending on the number of cycles [68]. In this study, it is assumed that environmental conditions, including temperature and pressure, are maintained at satisfactory levels to minimise their impact on ESS ageing. Additionally, for ESS types susceptible to lifespan reduction due to excessive DOD, such as batteries, the SOC is maintained within a reasonable range to prevent significant degradation and preserve the overall lifespan of the ESS.

3.5. Representation of uncertainty

This study identifies four key uncertain input variables in the standalone DC microgrid: solar irradiance, wind speed, offshore site load demand, and ambient temperature. PDFs for the weather-related variables are derived from 14 years of historical data obtained from New Zealand's NIWA website for the location of the proposed "Blue Endeavor" open ocean aquaculture farm by The New Zealand King Salmon Company Limited [69]. Load demand data, collected over two weeks in summer and two weeks in winter, is extrapolated to represent an entire year by assuming that the summer demand profile extends from October to March, while the winter profile spans from March to September. Fig. 8 illustrates the average daily demand of an aquaculture farm operated by The New Zealand King Salmon Company Limited during typical summer and winter days. This demand profile is projected over a period of 13 years using a second-order Markov chain model, based on the assumption that industrial load growth follows domestic

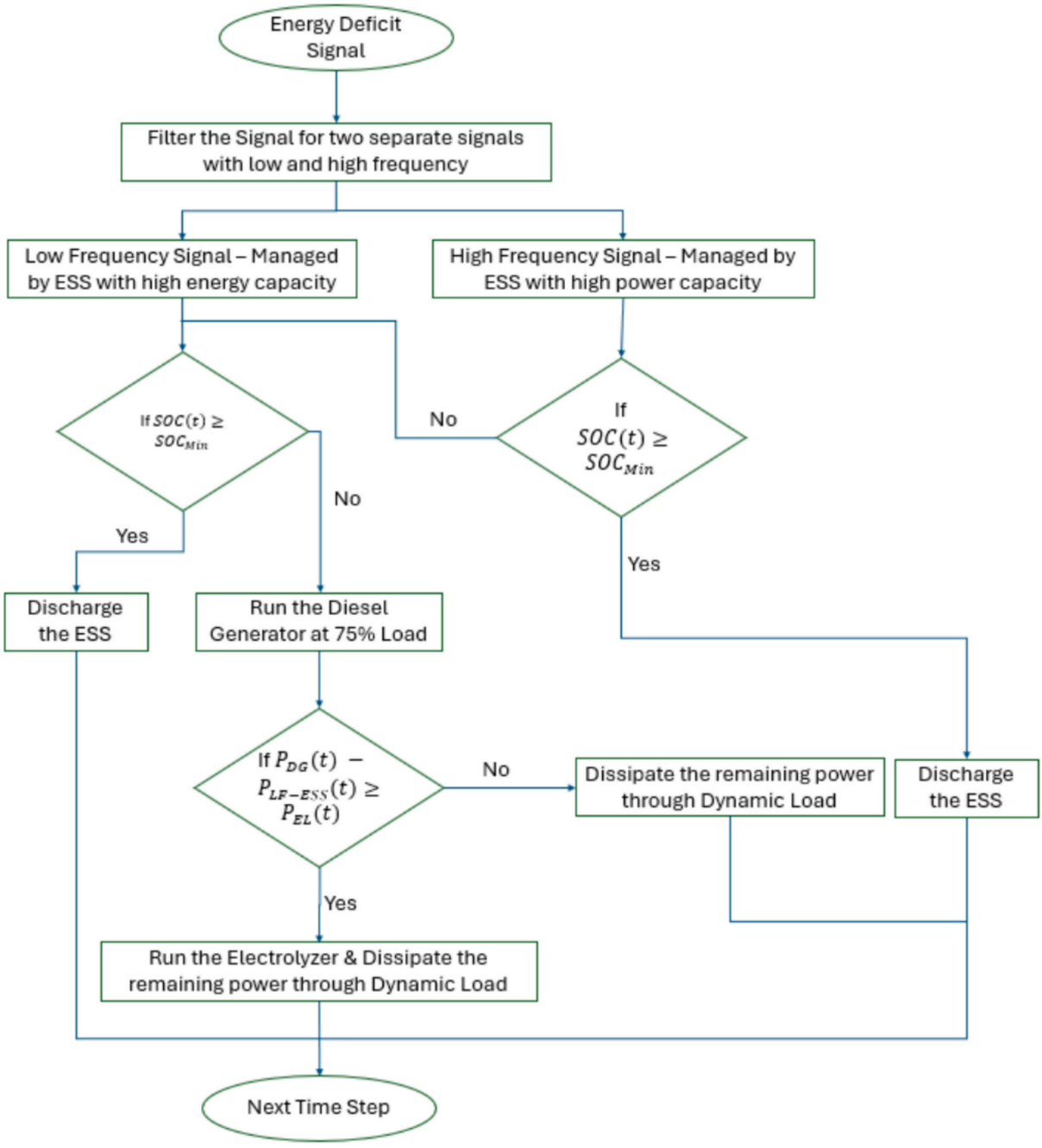

Fig. 5. Energy deficit management strategy.

consumption trends [70].

Scenario vectors were generated by permuting the uncertain input variables at 15-min intervals. The probabilities associated with these vectors were computed, as shown in Fig. 9, by dividing the Gaussian PDFs for load demand and ambient temperature into five discrete regions. This discretisation enabled the assignment of probabilities and corresponding input values to each scenario, which were calculated using Eqs. (50) and (51).

$$P_{X,Sc\ (n)} = \int_{x_{n-1}}^{x_n} PDF(X).dX, \forall Sc = 1, 2, .., n \tag{50}$$

$$E[X, Sc\ (n)\ ] = \frac{1}{P_{X,Sc\ (n)}} \int_{x_{n-1}}^{x_n} X.PDF(X).dX, \forall Sc = 1, 2, .., n \tag{51}$$

After discretising all uncertain variables into five scenarios, the total number of multi-dimensional scenarios for the optimisation problem reaches 625, resulting in a computationally intensive process. To address this challenge, a mixed integer linear programming (MILP)-based scenario reduction method, as described in [71], is employed. This method selects a minimal subset of scenarios that effectively represents the probability distributions of all four uncertain variables: solar irradiance, wind speed, ambient temperature, and load demand. The scenario reduction algorithm is mathematically formulated in Eq. (52), where N_{RSc} denotes the optimal number of reduced scenarios. The binary variable β_{Scn} indicates whether each original scenario is included,

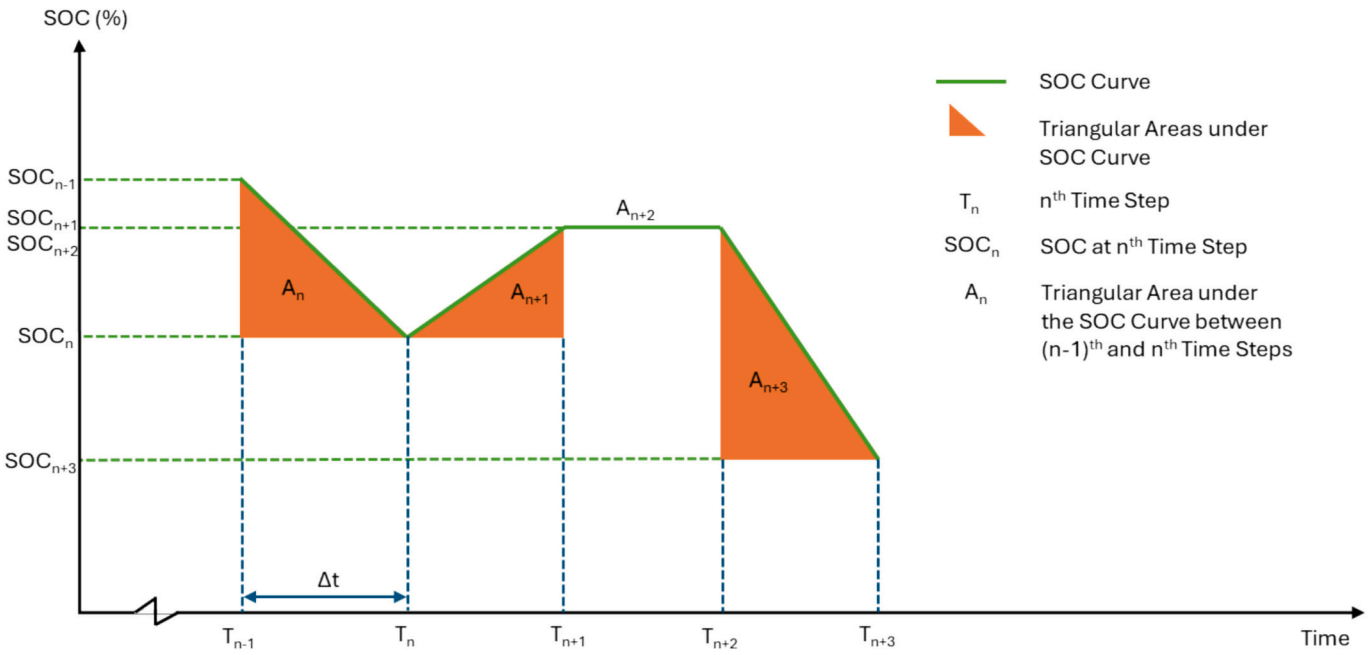

Fig. 6. Illustrative representation of cycle counting algorithm.

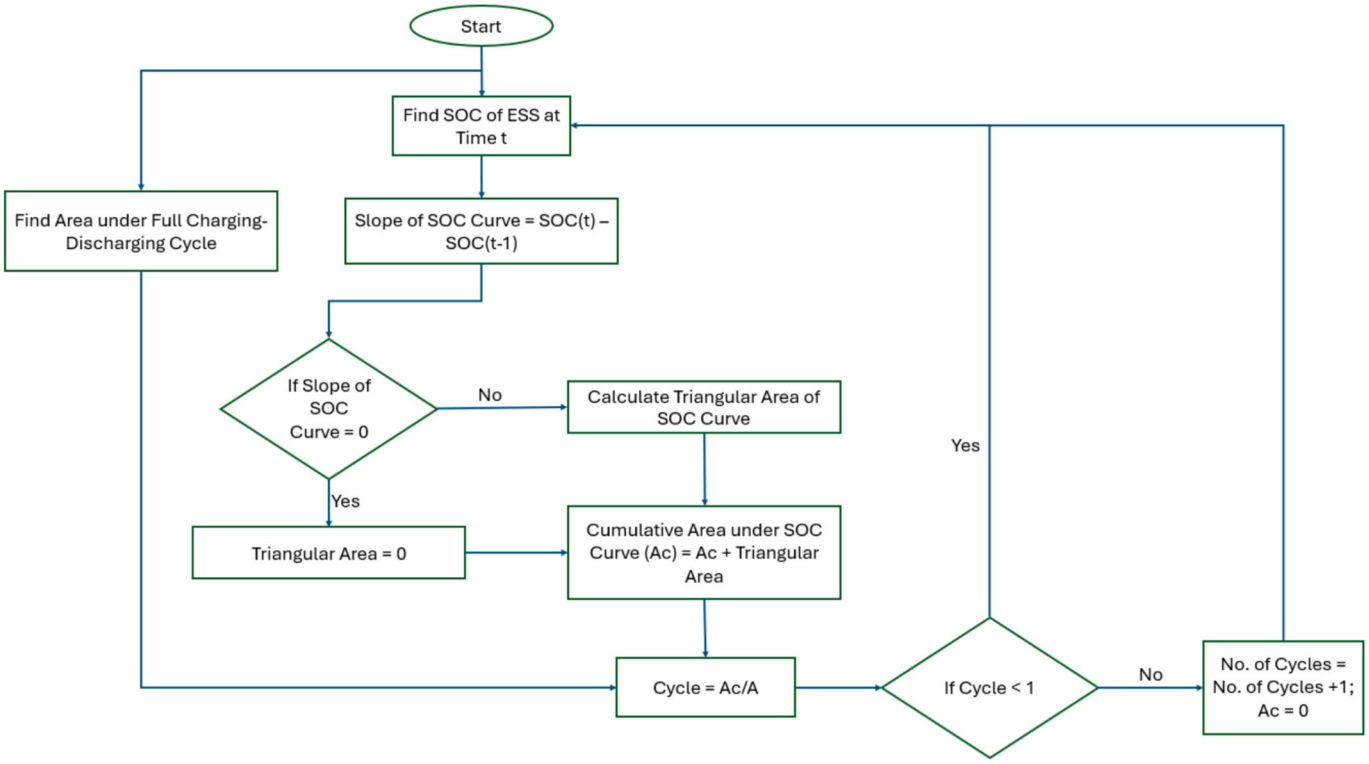

Fig. 7. Flowchart for the cycle counting algorithm.

subject to the constraints defined in Eqs. (53) and (54). The authors in [71] demonstrated through numerical examples that this scenario reduction approach yields solutions that are near optimal in terms of objective function values, even with a significantly reduced number of scenarios. Moreover, the resulting design variable values closely align with those obtained using the complete scenario set. This method has been successfully applied in analysis involving large datasets, including probabilistic studies of microgrids [72–74].

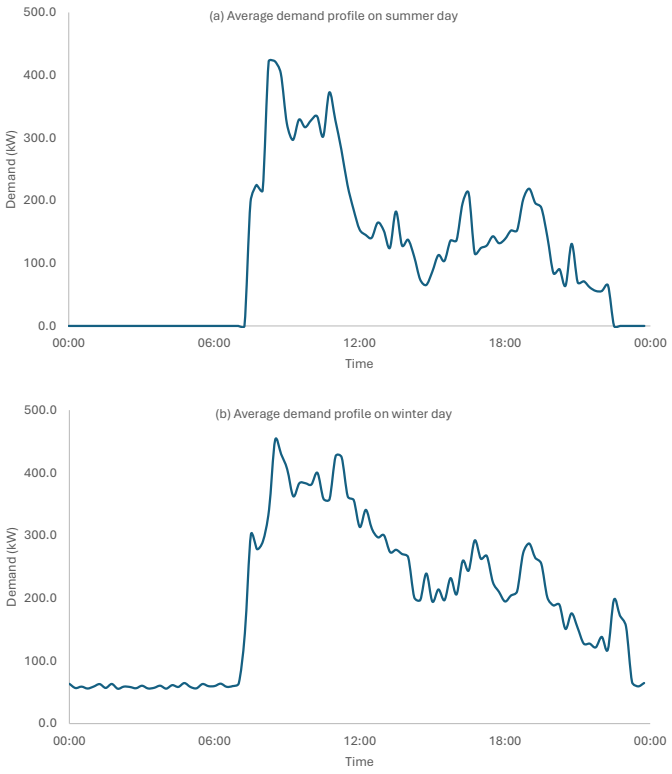

Fig. 8. Average demand profile of Te Pangu Aquaculture Farm of The New Zealand King Salmon Company Limited (a) Summer Day, (b) Winter Day.

$$N_{RSc} = \sum_{n=1}^{625} \beta_{Scn} \tag{52}$$

$$P(Sc_i) = \sum_{j=1}^{5}\sum_{k=1}^{5}\sum_{l=1}^{5} P(Sc_j, Sc_k, Sc_l), \quad \forall scenarios\ where\ i,j,k,l\ chosen\ from\ \{SI, WS, AT, LD\} \tag{53}$$

$$\sum_{i=1}^{5}\sum_{j=1}^{5}\sum_{k=1}^{5}\sum_{l=1}^{5} P(Sc_i, Sc_j, Sc_k, Sc_l) = 1, \forall scenarios\ where\ i,j,k,l\ chosen\ from\ \{SI, WS, AT, LD\} \tag{54}$$

3.6. Optimisation algorithm

The formulated optimisation problem can be effectively solved using various optimisation algorithms, with PSO being the primary method selected for this study. PSO has gained widespread adoption in power system research due to its simplicity, robustness, and adaptability. It is particularly effective for solving complex, nonlinear, non-convex, and multi-modal optimisation problems, which are common in applications such as economic dispatch, optimal power flow, and energy management in microgrids [75]. Unlike gradient-based methods, PSO does not require derivative information, making it suitable for non-differentiable or discontinuous problems frequently encountered in power system analysis [76].

PSO's capability to handle multi-objective optimisation, offering Pareto-optimal solutions for conflicting objectives such as cost minimisation and reliability enhancement, further strengthens its appeal. Its rapid convergence, scalability, and ability to manage continuous, discrete, or mixed-integer variables make it highly versatile [77]. Moreover, PSO can effectively accommodate uncertainties in power systems, including fluctuating renewable energy generation and variable load demands. Inspired by natural swarm behaviour, PSO simulates a population of candidate solutions (particles) that navigate the solution space, updating their positions based on both individual experiences and the experiences of neighbouring particles [78]. This mechanism enables PSO to deliver optimal or near-optimal solutions efficiently. Supported by extensive research and numerous algorithmic enhancements, PSO remains a preferred method for microgrid optimisation and broader power system applications.

Like other heuristic algorithms, PSO has certain drawbacks, such as susceptibility to local minima and an imbalance between exploration and exploitation [79]. To overcome these challenges, this study introduces a novel local search algorithm, QPSOL (Quadratic Programming Solver), integrated with PSO [80]. QPSOL enhances solution diversity and improves the balance between exploration and exploitation through a dynamic optimisation process. By employing quadratic interpolation (QI) around the optimal search agent, QPSOL improves solution accuracy and strengthens PSO's exploitation capability, thereby boosting the overall convergence efficiency of the algorithm.

The proposed optimisation strategy operates in two distinct phases within each generation. In the first phase, either PSO or QI is employed to update the positions of all particles. In the second phase, QPSOL is applied to enhance solution quality, refine particle positions, and promote efficient convergence. The population is subsequently ranked based on the fitness function and divided into two groups: QI is used to improve the performance of less optimal particles. At the same time, PSO explores the solution space around the best-performing particles.

To prevent excessive computation while maintaining exploitation capability, the local search in the proposed PSO–QPSOL framework is applied selectively rather than to all particles. A hybrid trigger condition is employed: local search is invoked when either the global best solution shows no improvement for a predefined number of iterations (stagnation detection), or the particle ranks within the top 10 % of the population. Once triggered, the local search operates within a fitness-driven adaptive radius, defined as $R(i)$, where α is a scaling factor, $F(i)$ is the fitness of particle i, and R_X denotes the decision variable bounds. This formulation ensures that particles closer to the global best undergo fine-grained exploitation with a smaller neighbourhood, while less-fit

particles explore a broader region. Such a design balances exploration and exploitation, enhances convergence speed, and avoids premature stagnation. The steps of the optimisation strategy are outlined in the pseudo code below.

Algorithm. PSO integrated with QPSOL and Extended Local Search.

1. Initialisation

(a) Initialise population P of N particles randomly within the feasible search space

(b) Initialise velocity V for each particle in P

(c) Set iteration counter $t = 0$

(d) Initialise stagnation counter $s = 0$

2. Main Loop

(e) While ($t < G_{Max}$) and ($Evaluations < E_{max}$)

Do:

3. Fitness Evaluation and Ranking

(f) For each particle i in P:

Evaluate the fitness of particle i $[F(i)]$

(g) Rank particles in P based on fitness values F

(h) Update global best G_B

If (G_B is improved) then $s = 0$

Else $s = s + 1$

4. Particle Update

(i) If (i belongs to the top 50% based on ranking):

I) Update particle's velocity using PSO rules:

$$V(i) = w.V(i) + c_1.r_1.[P_{Best}(i) - P(i)] + c_2.r_2.[G_{Best}(i) - P(i)]$$

II) Update particle's position:

$$P(i) = P(i) + V(i)$$

(j) Else (i belongs to the bottom 50%):

Update particle's position using QI Mechanism:

$$P(i) = QI[P(i)]$$

5. Local Search and Diversity Enhancement

(k) For selected particles:

If (($s \geq L$) OR (i in top 10% of ranked population)) then

Perform Local Search around $P(i)$ with radius $R(i)$

where $R(i) = \alpha.\left(1 - \frac{F(i)}{F(G_B)}\right).R_X$

(j) Apply binomial crossover to population P to increase diversity

6. Iteration Update

(k) Incremental Iteration Counter:

t = t + 1

(l) End While

7. Output Results

(m) Return the best solution found in population P

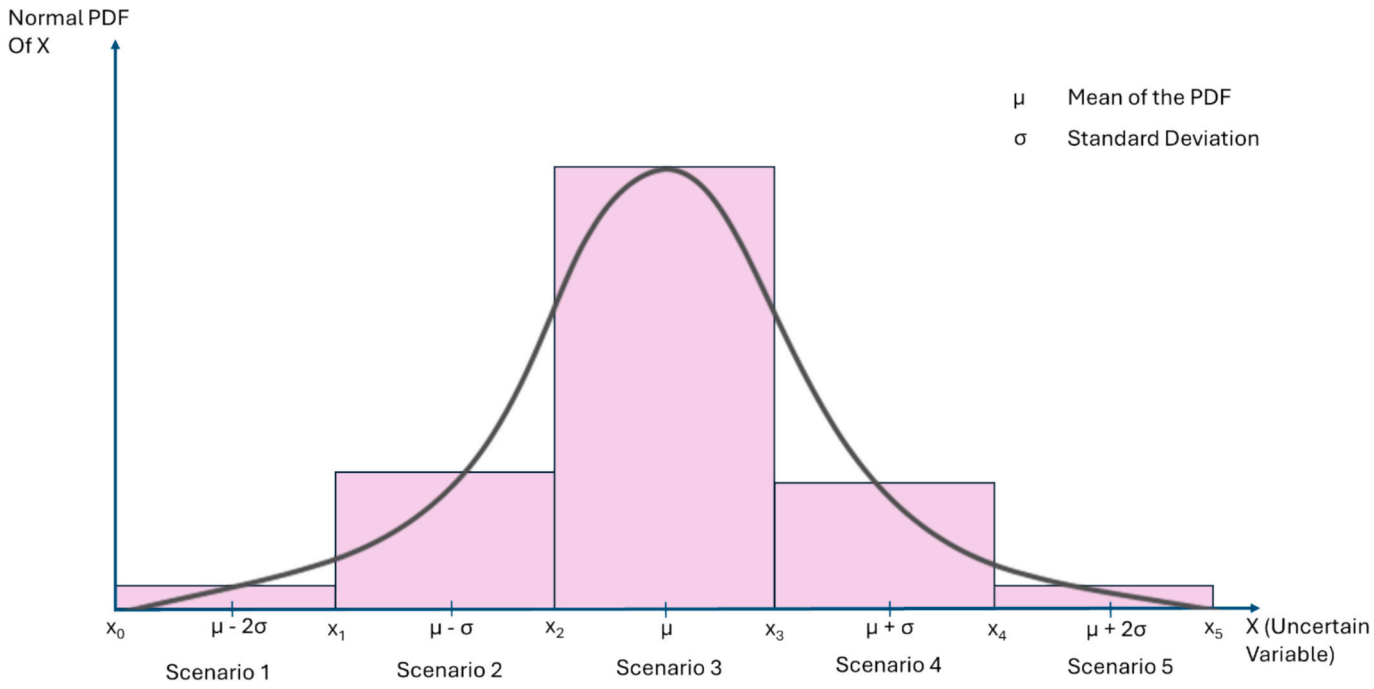

Fig. 9. PDF discretisation into scenarios: Gaussian Distribution (PDF is divided into intervals of equal size).

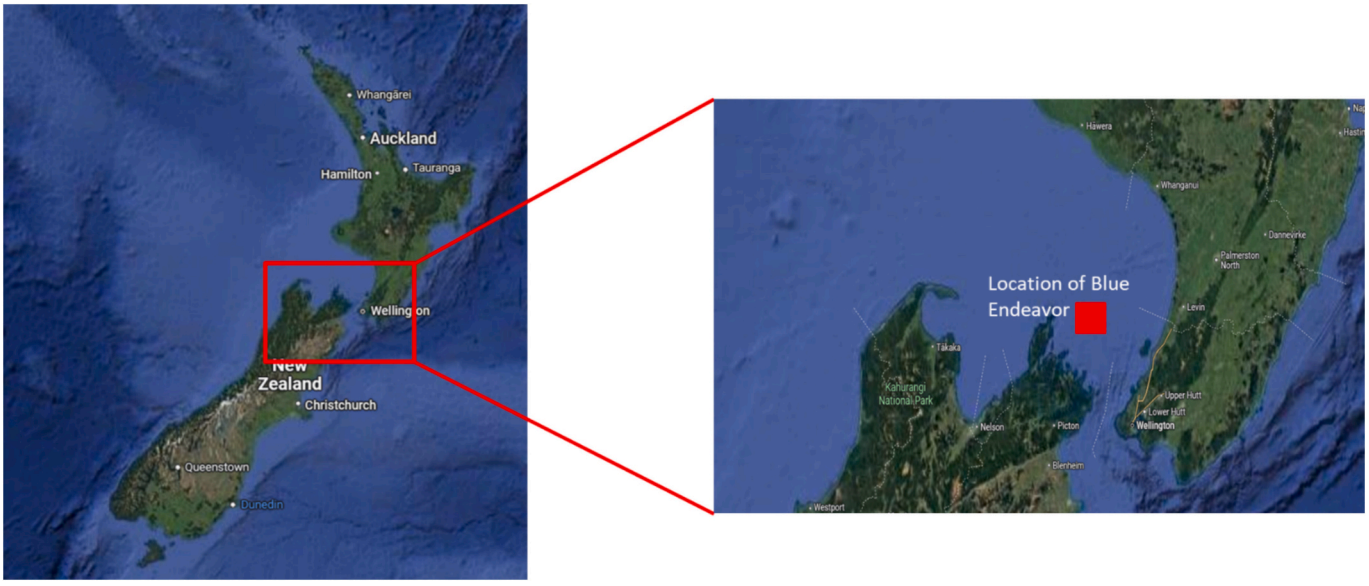

Fig. 10. Location of proposed blue endeavor farm (Image courtesy of Google Maps). (For interpretation of the references to colour in this figure legend, the reader is referred to the web version of this article.)

4. Case study: hydrogen-based standalone DC microgrid for offshore salmon aquaculture

The Blue Economy Cooperative Research Centre was established by the Australian Government to promote sustainable practices in offshore industries across Australia and New Zealand. Among its many initiatives is the development of open ocean aquaculture farms, which aim to increase fish yield per unit area [81]. To support the sustainable operation, transportation, and logistics of these farms, this study proposes transitioning to RES-powered infrastructure and hydrogen fuel cell-powered vessels [82]. The focus of this study is the design of an offshore standalone DC microgrid integrated with a hydrogen fuelling station to sustainably power aquaculture operations. The proposed microgrid will be located in Marlborough Sounds, New Zealand, where "Blue Endeavor," the country's first open-ocean salmon aquaculture farm, is currently under development [83]. Fig. 10 below shows the location of the proposed farm on Google Maps.

To develop the microgrid model for this case study, specific brands and equipment costs were selected based on the operational requirements of the salmon aquaculture farms. The technical specifications of the microgrid components are presented in Table 2, while the economic specifications, expressed in U.S. dollars, are detailed in Table 3. The microgrid is designed for a 25-year operational lifespan with an assumed interest rate of 6 %. Fig. 11 illustrates the monthly

Table 2
Technical Specifications of the proposed standalone microgrid.

Parameter	Value	Source	Parameter	Value	Source	Parameter	Value	Source
η_{PV}	22.6 %	[84]	C_P	0.5		L_{WC}	15 m	[85]
PR	80 %		A_{Swept}	397.6 m^2	[86]	$SOC_{BESS-Min}$	10 %	[87]
A_{Panel}	1.6 m^2		v_{in}	3.5 ms^{-1}		$SOC_{BESS-Max}$	90 %	
k	−0.29 % /^{0}C		v_{Rated}	10.5 ms^{-1}		SOC_{SC-Min}	5 %	[88]
T_{Ref}	25 °C		v_{out}	20 ms^{-1}		SOC_{SC-Max}	95 %	
η_{IG}	90 %	[86]	P_{Rated}	100 kW		η_{FC}	60 %	[89]
h_{CI}	0.5 m	[90]	h_{CO}	10.0 m	[90]			
η_{GB}	95 %		η_{WC}	40 %	[85]	η^{C}_{EL}	95 %	[91]
$P^{H_2}_{EL}$	700 bar	[92]	$P^{O_2}_{EL}$	13,790 kPa		d_{el}	5.1x10^{-4} µm	[93]
δ_{el}	1.15	[93]	a_x	1.2x10^{-5} cm	[94]	ΔH_{Vap}	241 kJ/mol	
P_{H_2O}	47.948 kPa		σ_{el}	0.137 s/cm		r_0	2.7x10^{-2} mΩ/cm^2	
P_o	4 bar		Q	0.95				

Table 3
Economic Specifications of the proposed standalone microgrid.

Parameter	Value	Unit	Source	Parameter	Value	Unit	Source
I_{PV}	1448	USD/kW	[95]	I_{BS}	1270	USD/kW	[95]
OM_{PV}	17.16	USD/kW-year		OM_{BS}	45.76	USD/kW-year	
I_{WT}	2098	USD/kW		I_{SC}	8300	USD/kW	
OM_{WT}	29.64	USD/kW-year		OM_{SC}	3.25	USD/kW-year	
I_{WC}	5934	USD/kW	[96]	I_{FC}	6771	USD/kW	[97]
OM_{WC}	41.25	USD/kW-year		OM_{FC}	34.65	USD/kW-year	
I_{DG}	700	USD/kW	[98]	I_{EL}	1520	USD/kW	[99]
OM_{DG}	33	USD/kW-year		OM_{EL}	25	USD/kW-year	
C_D	1.50	USD/Liter		I_{HT}	750	USD/kgH_2	
CT	70	USD/t-CO_2	[61]	OM_{HT}	15	USD/ kgH_2-year	

average 24-hour profiles of the uncertain variables over one year. For the probabilistic study, 14 years (2010−2023) of historical data on solar irradiance, wind speed, and ambient temperature were obtained from the NIWA website.

This study proposes the design of a standalone DC microgrid powered by RES to support an offshore facility equipped with a hydrogen fuel station. The strategy aims to minimise the microgrid's lifecycle cost through the integration of HESS. The following subsections present a detailed description of the proposed optimisation strategy, which incorporates a probabilistic approach to account for uncertainties in system inputs.

5. Simulation and results

The proposed optimisation model was developed and evaluated in MATLAB R2024a, using a one-year offshore demand profile with 15-min time intervals. Three energy storage configurations were analysed: (1) battery-only ESS, (2) battery combined with SCESS, and (3) hydrogen energy storage combined with SCESS. Each configuration was simulated under two scenarios: a deterministic simulation using one year of data, and a probabilistic simulation incorporating 14 years of historical data. Key outcomes from the probabilistic analysis support decision-making in microgrid design by identifying three lifecycle cost scenarios: best-case, average-case, and worst-case, corresponding to the 10th percentile, expected value, and 90th percentile of lifecycle cost results, respectively, based on a normal distribution. The boundaries for decision variables are provided in Table 4. For each scenario, 40 independent trial runs were performed, and the run yielding the lowest lifecycle cost was selected as the optimal solution for further analysis.

5.1. Scenario 1: battery only system

The battery-only ESS served as the baseline configuration for this optimisation study. No energy filter was applied, as there is no high-power capacity storage available to manage high-frequency demand fluctuations. A rule-based energy management algorithm was implemented, wherein excess renewable energy is used to charge the battery, and any demand exceeding the renewable generation is met through battery discharge. The initial optimisation was performed using one year of deterministic data for the uncertain variables.

In the probabilistic study, PSFs were generated for the uncertain variables using 14 years of historical weather data, along with synthetically generated demand profiles from the same period. The data were divided into five discrete segments to improve approximation accuracy. A total of 625 scenarios, resulting from the discretisation of these variables, were reduced to five using a scenario reduction algorithm based on MILP. Table 5 compares these five reduced scenarios with the deterministic data for a specific date, while Table 6 presents the optimisation results across different scenarios.

5.2. Scenario 2: battery + SC HESS

In this scenario, the BESS is combined with SCESS to form a HESS. The BESS manages the low-frequency component of the demand signal due to its high energy density. At the same time, the SCESS handles the high-frequency component due to its high power capacity. A second-order low-pass filter is employed to separate the demand signal into its respective frequency components. The deterministic and probabilistic data for this scenario were obtained using the same methodology as in Scenario 1 (battery-only scenario). The optimisation results for this scenario are presented in Table 7.

5.3. Scenario 3: hydrogen energy storage + SC HESS

The dynamic performance of fuel cells in microgrids is constrained by the oxygen and hydrogen feeding systems, making them unsuitable for managing rapid power demand fluctuations. These limitations can result in voltage drops, leading to increased stress on power converters, frequent fuel cell switching, voltage instability, and a reduced lifespan for both fuel cells and converters [100]. Due to these challenges, hydrogen energy storage alone is not ideal for ESS in applications with frequent power variations. To address rapid fluctuations, a secondary ESS is required. While batteries can fulfil this role, their lower power handling capacity makes them less optimal. High-power capacity

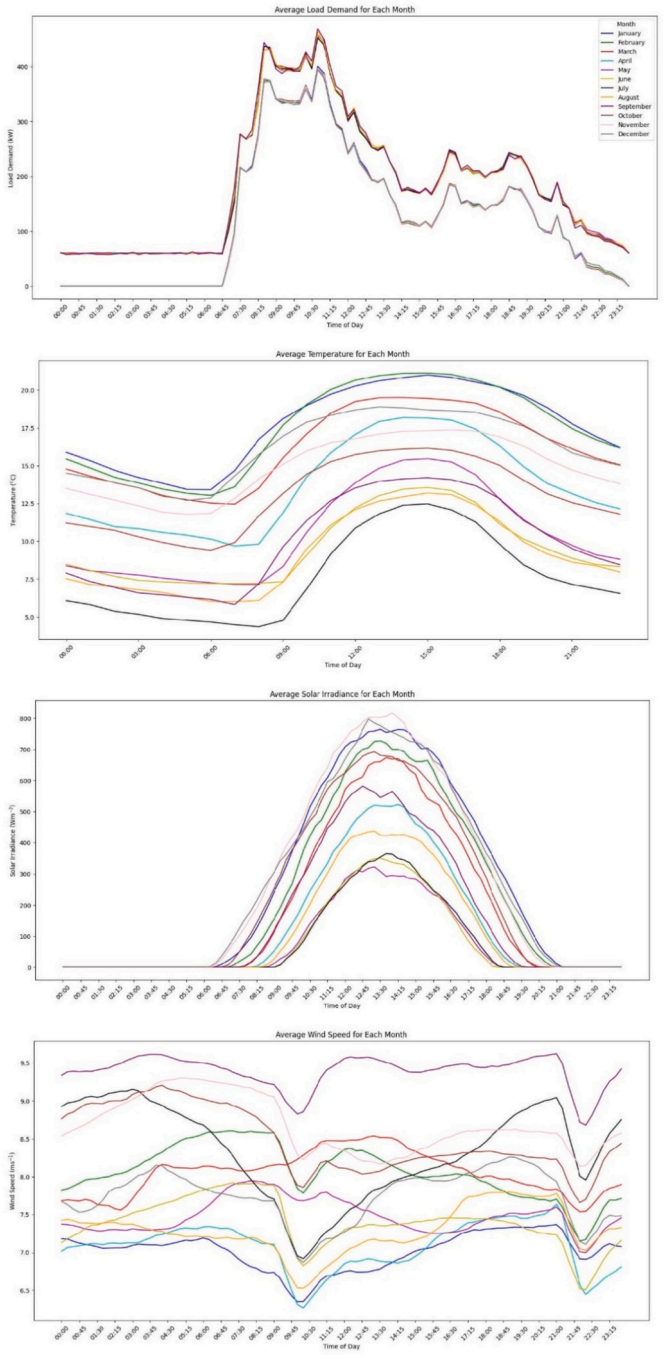

Fig. 11. Monthly average 24-hour profiles for uncertain variables: Solar irradiance, Wind speed, Temperature, Load Demand.

systems, such as supercapacitors, offer a more effective solution for managing rapid power variations in hydrogen energy storage-based microgrids [101].

In this study, hydrogen energy storage and SCESS were evaluated as a HESS. Similar to Scenario 2, a second-order low-pass filter was used to separate the demand signal into low- and high-frequency components, which were managed by the fuel cell and SCESS, respectively. As the fuel cell has a ramp up rate in switching, SCESS supports the fuel cell for few seconds until fuel cell can absorb the total power requirement. For both deterministic and probabilistic studies, the data were obtained by discretising the PDFs and applying a scenario reduction algorithm. In this scenario, the hydrogen required for the fuel cell is supplied directly by the PEM electrolyser, thereby increasing the load demand on the microgrid. The results of the optimisation for this configuration are presented in Table 8.

Table 4
Upper and lower boundaries for the decision variables of the optimisation problem.

Decision variable	Lower boundary (LB)	Upper boundary (UB)	Selection criteria
N_{PV}	0	* 2140 * 2720: Scenario 3 (With fuel cell)	UB: Number required to meet demand with 4 h of peak sunlight.
N_{WT}	0	* 14 * 17: Scenario 3 (With fuel cell)	UB: Number required to meet demand through wind energy.
N_{WC}	0	* 15 * 18: Scenario 3 (With fuel cell)	UB: Number required to meet demand through wave energy.
P_{DG}	630 kW 0: Scenario 3 (With fuel cell)	2480 kW	LB: Capacity needed for meet demand with 5 % LOLP at 75 % load without hydrogen production. UB: Capacity required to meet the peak demand with a 15 % margin with hydrogen production (8 h electrolyser at 75 % load).
E_{BS}	0	5935 kWh	UB: Capacity to supply half the daily demand.
E_{SC}	0	405 kWh	UB: Capacity for peak demand during hydrogen production over 15 min.
P_{FC}	0	1350 kW	UB: Capacity to supply half the peak demand with 8 h of full-load hydrogen production.
P_{EL}	370 kW	1700 kW	LB: Capacity to meet fuel station needs with 24-h operation. UB: Capacity to meet both fuel station and fuel cell needs with 8-h operation.
m_{HT}	200 kg	500 kg	LB: Capacity to store hydrogen for the fuel station. UB: Capacity to store daily hydrogen for the fuel station and fuel cell.

5.4. Comparison of the results of three scenarios

The results from the three evaluated scenarios reveal several key insights. Notably, wave energy was excluded from the optimal design scenarios in all scenarios, indicating that, given the current costs of wave energy converters and associated infrastructure, wave energy remains economically uncompetitive compared to more established RES like solar PV and wind, even for offshore standalone DC microgrids. From an economic perspective, solar PV and wind continue to be the preferred RES options for microgrid design.

The lowest LCOE was achieved with the battery + SC HESS, showing an 11.14 % reduction compared to the baseline battery-only system. This reduction occurred despite the per-unit cost of SCESS being more than seven times that of BESS. Two key factors contributed to this improvement.

1. Reduced BESS Capacity Requirement: In the battery + SC configuration, the required BESS capacity decreased by approximately 47 %, from 5100 to 5250 kWh in the battery-only system to 2700–3000 kWh.
2. Extended BESS Replacement Frequency: The replacement period for BESS increased from 11.5 years in the battery-only scenario to 17 years when coupled with an SC, thereby reducing overall replacement costs.

Table 5
Comparison of Deterministic and Probabilistic Study Values for uncertain variables at 12:00 Noon on January 1st.

Study	Scenario	Probability of Occurrence	Solar Irradiance (W/m^2)	Wind Speed (m/s)	Ambient Temperature (°C)	Load Demand (kW)
Deterministic	N/A	N/A	937.3	6.9	18.6	297.1
Probabilistic	1	0.275	847.2	7.7	20.1	313.3
	2	0.223	983.7	8.9	17.7	289.0
	3	0.202	711.4	9.8	19.2	297.0
	4	0.154	653.9	10.3	19.3	301.0
	5	0.146	572.4	9.2	18.4	293.2

Table 6
Results for optimisation problem for Scenario 1 – Battery only system.

Output of Optimisation Problem	Deterministic Study	Probabilistic Study		
		Best Case	Average Case	Worst Case
Total Cost of microgrid (USD Millions)	23.92	22.01	24.74	28.65
LCOE (US Cents/kWh)	22.09	20.32	22.84	26.45
Carbon Footprint ($tCO_{2,eq}$)	14,392	11,247	14,553	15,018
Replacement Frequency of ESS (Years)	BESS – 11.5	BESS – 12	BESS – 11.5	BESS – 11.5
N_{PV}	2129	2116	2131	2143
N_{WT}	10	9	10	11
N_{WC}	0	0	0	0
P_{DG} (kW)	630	630	630	650
E_{BS} (kWh)	5150	5100	5150	5250
P_{EL} (kW)	580	550	590	620
m_{HT} (kg)	200	200	200	200

Table 7
Results for optimisation problem for Scenario 2 – Battery + Supercapacitor system.

Output of Optimisation Problem	Deterministic Study	Probabilistic Study		
		Best Case	Average Case	Worst Case
Total Cost of microgrid (USD Millions)	21.27	19.79	21.70	24.04
LCOE (US Cents/kWh)	19.63	18.28	20.04	22.19
Carbon Footprint ($tCO_{2,eq}$)	10,256	8133	10,810	12,014
Replacement Frequency of ESS (Years)	BESS – 17 SCESS – No	BESS – 17 SCESS - No	BESS – 17 SCESS - No	BESS – 16.5 SCESS - No
N_{PV}	2129	2114	2129	2141
N_{WT}	10	9	10	11
N_{WC}	0	0	0	0
P_{DG} (kW)	630	630	630	650
E_{BS} (kWh)	2830	2720	2850	2950
E_{SC} (kWh)	120	110	120	135
P_{EL} (kW)	580	550	590	620
m_{HT} (kg)	200	200	200	200

Due to these factors, the LCOE of the battery + SC system was lower than that of the battery-only system, even with the additional cost of SCESS.

Furthermore, compared to the hydrogen energy storage + SC HESS, the battery + SC system achieved a 42.69 % reduction in LCOE. The higher costs associated with fuel cells and their lower efficiency contributed to this high LCOE for the hydrogen energy storage + SC HESS.

In the probabilistic study, across all scenarios (best-case, average-case, and worst-case), the battery + SC HESS consistently demonstrated a significant reduction in LCOE compared to both the battery-only and hydrogen energy storage + SC configurations. Fig. 12 illustrates a comparative overview of LCOE values for the three scenarios in both deterministic and probabilistic studies.

Table 8
Results for optimisation problem for scenario 3 – hydrogen energy storage + SC system.

Output of optimisation problem	Deterministic study	Probabilistic study		
		Best case	Average case	Worst case
Total Cost of microgrid (USD Millions)	47.07	42.75	49.49	56.63
LCOE (US Cents/kWh)	34.25	31.12	36.03	41.23
Carbon Footprint ($tCO_{2,eq}$)	0	0	0	0
Replacement Frequency of ESS (Years)	Fuel cell - No SCESS - No	Fuel cell - No SCESS - No	Fuel cell - No SCESS - No	Fuel cell - No SCESS - No
N_{PV}	2669	2629	2701	2731
N_{WT}	14	13	15	17
N_{WC}	0	0	0	0
P_{DG} (kW)	0	0	0	0
E_{SC} (kWh)	175	170	185	195
P_{FC} (kW)	1250	1175	1275	1350
P_{EL} (kW)	950	920	970	1020
m_{HT} (kg)	350	310	350	390

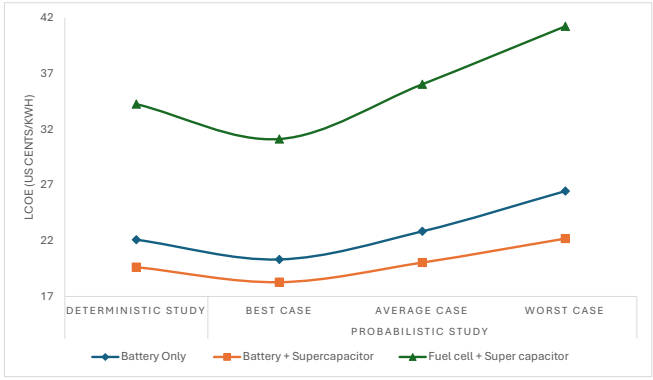

Fig. 12. Comparison of LCOE for three ESS scenarios: deterministic study vs. probabilistic study.

A standalone DC microgrid powered solely by a diesel generator typically has a minimum LCOE of approximately 30 US cents/kWh [102]. In contrast, renewable energy-based microgrids, whether using a battery-only system or a battery + SC HESS, offer significant cost advantages, making them economically superior to diesel-only systems. However, the hydrogen energy storage + SC HESS, when integrated into a renewable energy microgrid, remains less competitive than diesel-powered systems due to the high costs associated with fuel cells and electrolysers. Even in scenarios where an electrolyser is already available for hydrogen production, or where carbon taxes are imposed on diesel operations, the economic performance of the hydrogen energy storage + SC system remains unfavourable. This is primarily due to the high capital costs and lower efficiency of current fuel cell and electrolyser technologies.

Despite these economic challenges, the hydrogen energy storage + SC system offers the benefit of eliminating diesel usage, thereby reducing the microgrid's carbon footprint to zero. If fuel cell and electrolyser costs decline significantly and efficiencies improve, this system could become a viable solution for green offshore microgrids in the future. Fig. 13 illustrates the variation in LCOE for a hydrogen energy storage + SC HESS integrated microgrid as the fuel cell costs decrease, with efficiency levels maintained at 60 % and increased to 75 %. The results indicate that:

- When fuel cell efficiency is maintained at 60 %, the LCOE of the hydrogen energy storage + SC HESS falls below that of the battery + SC HESS once the fuel cell cost reaches 1981 USD/kW.
- If the fuel cell efficiency increases to 75 %, this LCOE crossover occurs at 2078 USD/kW.

This means that, with current cost levels, the fuel cell price would need to decrease by 70.7 % to achieve cost parity with the battery + SC HESS without efficiency improvements. If the fuel cell efficiency increases to 75 %, the required cost reduction is slightly lower at 69.3 %.

To further assess the effectiveness of the battery + SC HESS compared to the battery-only configuration, an analysis of the power curves, presented in Fig. 14, provides valuable insights. The charging curve of the BESS is notably smoother in the battery + SC HESS than in the battery-only configuration. The SCESS absorbs power peaks, effectively mitigating power surges in the battery's charging curve. This has resulted in a lower required capacity for the BESS and significantly

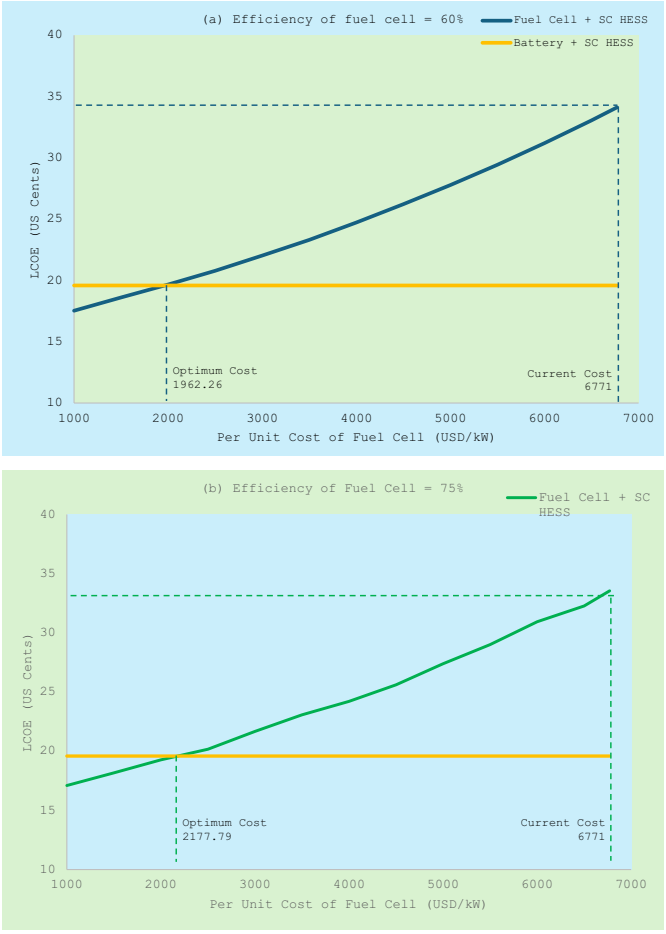

Fig. 13. LCOE variation of hydrogen energy storage + SC HESS integrated microgrid with the change of the cost of fuel cell [(a) Efficiency kept at 60 %, (b) Efficiency increased up to 75 %.

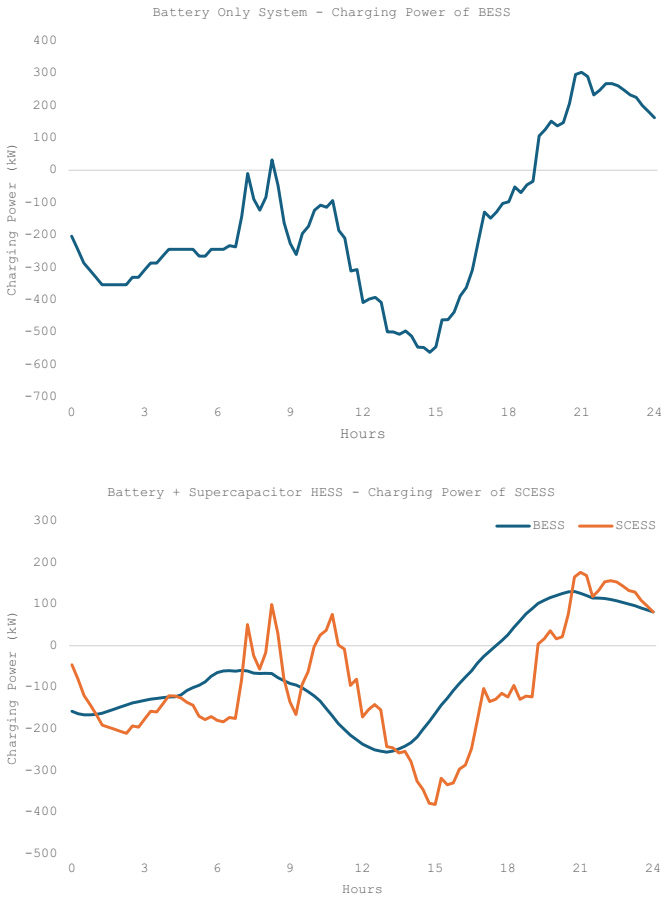

Fig. 14. Charging-discharging curve for BESS for Scenario 1 & Scenario 2, and Charging curve for SCESS for Scenario 2.

reduced the number of charge-discharge cycles necessary for daily operation.

In this design, hydrogen production for both the fuel cell and the hydrogen fuelling station was powered entirely by RES, resulting in the generation of green hydrogen across all three scenarios. Scenarios 1 and 2 include only the hydrogen fuelling station, while scenario 3 incorporates both a fuel cell and a hydrogen fuelling station. Notably, except for Scenario 3, which utilises hydrogen energy storage + SC HESS, producing green hydrogen from RES proved to be more cost-effective than relying on fossil fuels for hydrogen production in the offshore standalone DC microgrid. Fig. 15 illustrates the electrolyser's operational profile, averaged over a summer and winter day, for Scenarios 2 and 3. The load demand profiles for the electrolyser in Scenario 1 and Scenario 2 are nearly identical. From both figures, it is evident that during summer, the electrolyser load peaks during daylight hours, coinciding with maximum solar PV generation. In contrast, during winter, the load peaks from midnight to early morning, aligning with lower demand periods when wind power serves as the primary energy source.

The key insights from analysing the electrolyser demand profiles include:

✓ Optimum size of the electrolyser is determined mainly by green hydrogen production during the daytime in summer, utilising both solar PV and wind energy as RES. This is evident from the consistently high electrolyser output throughout summer, as shown in the average profiles.

✓ Minimum hydrogen production occurs in the evening when renewable energy generation is low, and load demand is high in both

Fig. 15. Electrolyser average demand profile for summer and winter for Scenario 2 and Scenario 3.

seasons. This is particularly clear in the summer demand profile. In winter, reduced hydrogen production during the day is also observed due to lower solar irradiance, limiting PV generation compared to summer.

✓ Higher hydrogen production rates are seen from midnight to early morning, when offshore site load demand is significantly lower. In winter, this production is notably higher than in summer, due to comparatively lower daytime generation.

Fig. 16 provides a comparative analysis of optimisation results under different uncertainty budgets, highlighting the significance of probabilistic modelling in standalone microgrid design. The key insights are:

✓ **Best Case Scenario**: In the most optimal scenario for the battery + supercapacitor HESS, the Levelized Cost of Energy (LCOE) decreases by 7.0 % compared to the deterministic model. In contrast, the other two scenarios show a nearly 10 % increase in LCOE. This

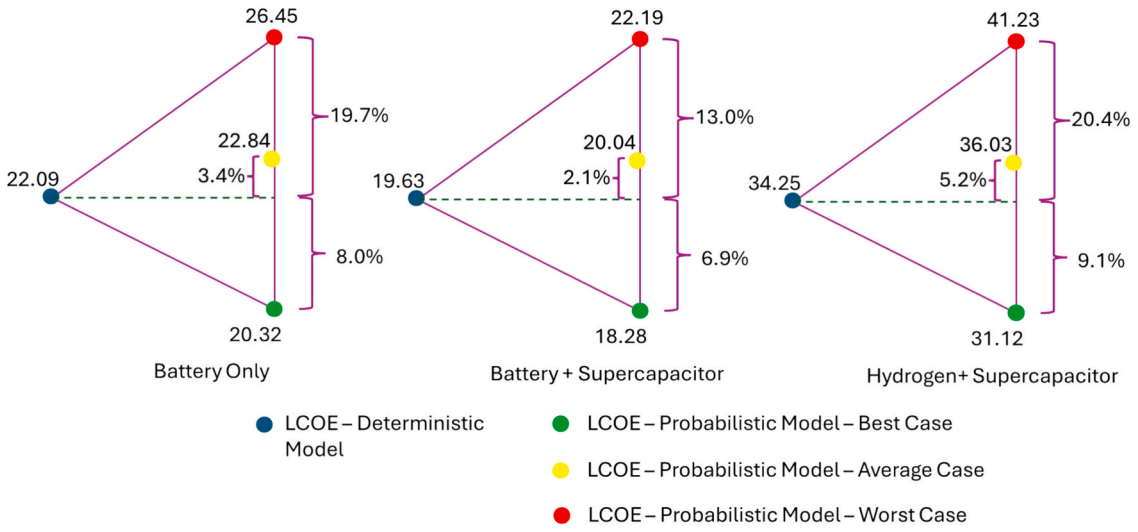

Fig. 16. Comparative analysis of probabilistic study under different uncertainty budgets.

demonstrates that significant savings can be achieved with a high-risk, cost-optimised design for the standalone microgrid using the battery + supercapacitor HESS.

✓ **Average Case Scenario**: Across all scenarios, the average-case scenario from the probabilistic study shows a slight increase in LCOE compared to the deterministic model. This rise is primarily due to the larger energy storage capacity required. The probabilistic study offers a more robust understanding of the optimal design, accounting for uncertainties in standalone microgrid design.

✓ **Worst Case Scenario**: The worst-case scenario shows a 12.9 % increase in LCOE compared to the deterministic model. For the battery-only system and the hydrogen energy storage + supercapacitor HESS, the LCOE rises significantly by 19.8 % and 20.3 %, respectively. This suggests that, under critical conditions, a higher investment in generation and storage is required. Nevertheless, the battery + supercapacitor HESS still offers a more favourable LCOE than the other configurations and the diesel generator standalone system.

To evaluate the target cost of integrating wave energy into offshore standalone DC microgrids, the optimal standalone DC microgrid configuration with a battery–SC HESS was analysed under scenarios of reduced WEC costs and improved WEC efficiencies. Fig. 17 illustrates the number of WECs in the optimal design as a function of the unit cost of wave energy, considering the current efficiency of 40 % and hypothetical increases up to 80 %. The results indicate that, at the current efficiency level, the unit cost of wave energy must decrease by at least

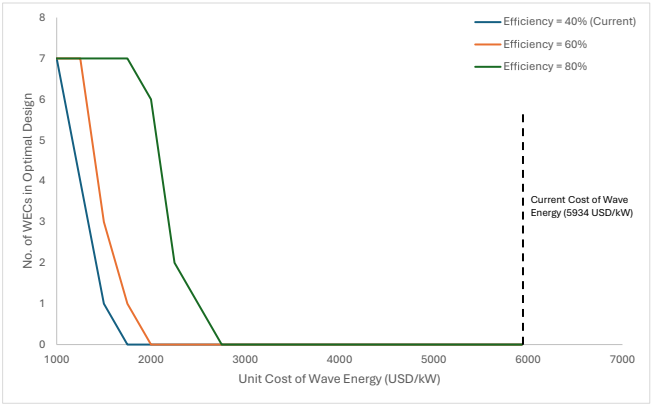

Fig. 17. Integration of wave energy in optimal design of standalone DC microgrid against the cost of wave energy under different efficiency levels.

70 % relative to present levels to achieve integration. Furthermore, even with efficiency improvements up to 80 %, a cost reduction of at least 58 % is required. These findings imply that, although wave energy shows promise, substantial cost reductions are essential for its integration into offshore standalone DC microgrids.

5.5. *Sensitivity analysis of key cost drivers*

To evaluate the impact of potential cost reductions in RES equipment and ESS, as well as increases in diesel generator fuel costs, on the optimal design of a standalone DC microgrid, further optimisations were conducted under three distinct scenarios: (1) Existing scenario: Current cost conditions are maintained throughout the microgrid's operational lifetime, (2) Realistic change scenario: The costs of RES and ESS equipment are reduced by 20 %, while diesel fuel costs are increased by 20 %, (3) Extreme change scenario: The costs of RES and ESS equipment are reduced by 70 %, and diesel fuel costs are increased by 70 %. The results of these three scenarios are summarized in Table 9.

Model Output	Existing Scenario	Realistic Change Scenario	Extreme Change Scenario
Total Cost of microgrid (USD Millions)	21.27	18.09	11.37
LCOE (US Cents/kWh)	19.63	16.67	10.50
Carbon Footprint ($tCO_{2,eq}$)	10,256	3484	0
N_{PV}	2129	2375	2540
N_{WT}	10	13	15
N_{WC}	0	0	0
P_{DG} (kW)	630	630	630
E_{BS} (kWh)	2830	2980	3220
E_{SC} (kWh)	120	145	170
P_{EL} (kW)	580	580	580
m_{HT} (kg)	200	200	200

Table 9
Comparison of Average No. of iterations and time taken for convergence in different metaheuristic optimisation techniques.

Optimisation Algorithm	Average CPU Usage Time until convergence (s)	Average No. of Iterations for Convergence	Average CPU Usage Time for one iteration (s)
GA	7189	127	56.61
ACO	6543	117	55.92
Standard PSO	6671	110	60.65
Enhanced PSO (This study)	6310	93	67.84

Based on the data presented in Table 9, a 20 % reduction in RES and ESS costs combined with a 20 % increase in diesel fuel prices results in a significant decrease, approximately 66 %, in diesel generator utilisation, as reflected in the corresponding reduction in carbon footprint. Under the extreme scenario, where RES and ESS costs are reduced by 70 % and fuel costs are increased by 70 %, the diesel generator is not utilised at all. In this case, the RES and ESS systems fully meet the microgrid's energy demand. The LCOE decreases by 15 % in the realistic scenario and by 46.5 % in the extreme scenario. This reduction in diesel generator usage is primarily attributed to the increased ESS capacity enabled by lower costs, which allows the system to store and supply energy that would otherwise require diesel generation. Additionally, the capacity of RES is expanded in conjunction with ESS, as the enhanced storage capability facilitates greater integration of renewable energy. These findings suggest that substantial cost reductions in RES and ESS technologies can enable standalone DC microgrids to operate entirely on renewable energy. This is a key observation and a significant conclusion drawn from the analysis.

5.6. Sensitivity analysis of quality factor of the low pass filter

In the design of the standalone DC microgrid, a low-pass filter quality factor of 0.9 was assumed for computational convenience. To assess its impact on the lifecycle cost of the microgrid, different quality factor values were evaluated under the deterministic optimal design scenario of the standalone DC microgrid integrating a battery–supercapacitor HESS. Fig. 18 illustrates the variation of the LCOE with respect to the quality factor. The results show that a higher quality factor generally reduces the lifecycle cost. However, in practical applications, a quality factor close to unity implies that signals near the cutoff frequency are split between the two ESS units [103]. In the presence of noise, harmonics, and sensor errors, such conditions can lead to oscillations. Therefore, the selected value of 0.9 is considered more appropriate, as it balances lifecycle cost minimization with system stability.

6. Performance analysis of the proposed methodology

This study introduces a set of novel methodologies aimed at optimising the lifecycle cost of standalone DC microgrids for offshore applications. The computational and statistical performance of these methodologies, applied at various stages of the optimisation process, is evaluated and compared against existing techniques. The following subsections present a detailed analysis of each method's performance, highlighting improvements in efficiency, accuracy, and robustness over conventional approaches.

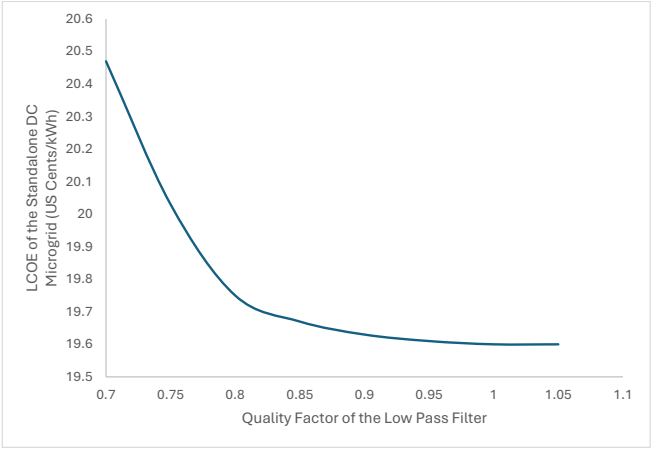

Fig. 18. Variation of lifecycle cost of the microgrid with the quality factor of the low pass filter of HESS.

6.1. Performance analysis of the proposed enhanced PSO

The proposed enhanced PSO algorithm was executed for 40 independent runs on the dataset, with each run consisting of up to 200 iterations. From these runs, the best and worst cases were identified based on the lowest and highest lifecycle costs of the microgrid, respectively. To evaluate the performance of the enhanced PSO algorithm, the same procedure was applied using three widely adopted metaheuristic optimisation techniques: GA, ACO, and standard PSO. These comparisons were conducted using the most optimal deterministic scenario: Scenario 2, which incorporates a battery + SC HESS. The best and worst runs from each of the four optimisation techniques are plotted and compared in Fig. 19, providing a visual assessment of their relative performance in minimising lifecycle cost.

From above figures, several key observations can be made. First, the selected number of iterations (i.e., 200) is sufficient to ensure convergence for each algorithm. Second, the enhanced PSO algorithm clearly outperforms the established metaheuristic techniques; GA, ACO, and standard PSO, in terms of minimising lifecycle cost. These results demonstrate that the enhancements introduced to the PSO algorithm, specifically the integration of quadratic interpolation and extended local search mechanisms, significantly improve its efficiency and effectiveness in standalone DC microgrid sizing applications.

CPU time required for convergence is another important metric for evaluating the performance of the proposed optimisation algorithm [104]. Table 9 presents a comparative overview of the average convergence time for each algorithm applied to the deterministic model of the optimisation problem. The results indicate that the proposed enhanced PSO algorithm outperforms the other metaheuristic techniques, GA, ACO, and standard PSO, in terms of average CPU time to

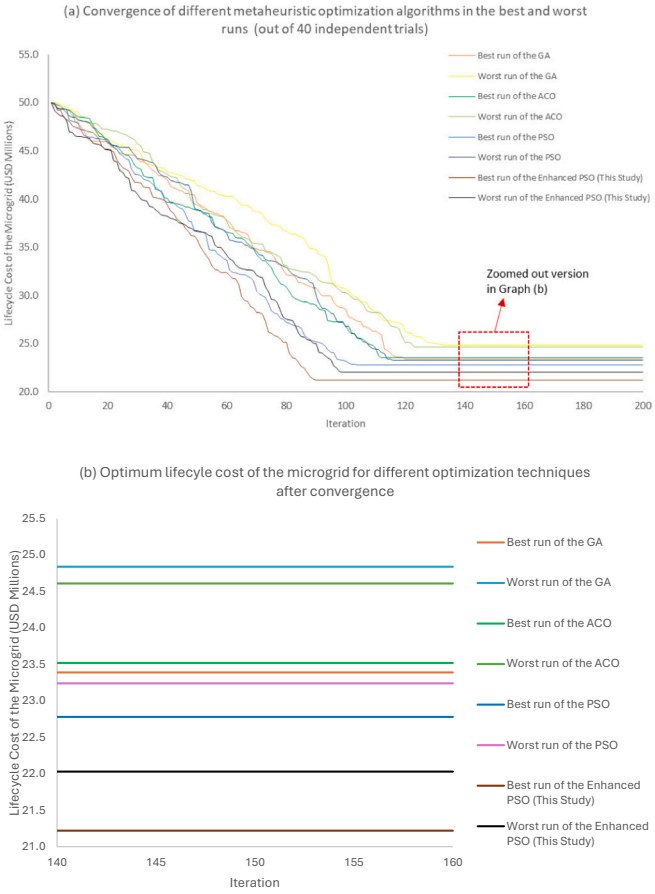

Fig. 19. Comparison of convergence of proposed enhanced PSO algorithm with three common metaheuristic optimisation techniques.

Table 10
Statistical parameters of the 40 independent trials of proposed enhanced PSO.

Output (F_i)	Best (F_{Best})	Worst (F_{Worst})	Mean ($F_{Mean} = \frac{\sum_{i=1}^{N} F_i}{N}$)	SD $\left(\sqrt{\frac{\sum_{i=1}^{N}(F_i - F_{Mean})^2}{N-1}}\right)$	RMSE $\left(\sqrt{\frac{\sum_{i=1}^{N}(F_i - F_{Best})^2}{N}}\right)$	RE $\left(\frac{\sum_{i=1}^{N} F_i - F_{Best}}{F_{Best}}\right)$
Lifecycle Cost of the Microgrid (USD Millions)	21.22	22.03	21.67	0.201	0.203	0.0227
LCOE (US Cents)	19.59	20.34	20.01	0.188	0.191	0.0107
Carbon Footprint ($tCO_{2,eq}$)	10,245	10,713	10,449	117	118	0.0143

Table 11
Descriptive Statistics for Cycle Time in different ESS, for (a) Proposed ESS degradation algorithm, (b) Rainflow counting algorithm.

(a) Proposed ESS Degradation Algorithm:

Output (F_i)	Best (F_{Best})	Worst (F_{Worst})	Mean ($F_{Mean} = \frac{\sum_{i=1}^{N} F_i}{N}$)	SD $\left(\sqrt{\frac{\sum_{i=1}^{N}(F_i - F_{Mean})^2}{N-1}}\right)$	RMSE $\left(\sqrt{\frac{\sum_{i=1}^{N}(F_i - F_{Best})^2}{N}}\right)$	RE $\left(\frac{\sum_{i=1}^{N} F_i - F_{Best}}{F_{Best}}\right)$
Number of cycles per year for BESS	520	533	525	3.25	3.25	0.0057
Number of cycles per year for SCESS	35,454	35,529	35,497	18.75	18.76	0.00076

(b) Rainflow Counting Algorithm:

Output (F_i)	Best (F_{Best})	Worst (F_{Worst})	Mean ($F_{Mean} = \frac{\sum_{i=1}^{N} F_i}{N}$)	SD $\left(\sqrt{\frac{\sum_{i=1}^{N}(F_i - F_{Mean})^2}{N-1}}\right)$	RMSE $\left(\sqrt{\frac{\sum_{i=1}^{N}(F_i - F_{Best})^2}{N}}\right)$	RE $\left(\frac{\sum_{i=1}^{N} F_i - F_{Best}}{F_{Best}}\right)$
Number of cycles per year for BESS	538	559	554	5.25	5.25	0.0072
Number of cycles per year for SCESS	35,790	36,451	36,210	165.25	165.33	0.0058

convergence. Although each iteration of the enhanced PSO algorithm requires slightly more computational time than the others, the total number of iterations needed for convergence is significantly lower. This trade-off results in overall faster convergence and improved computational efficiency. These findings suggest that the enhanced PSO algorithm is a more effective and efficient tool for optimising the design of standalone DC microgrids.

To assess the robustness of the proposed enhanced PSO algorithm, statistical analysis was performed on the results from 40 independent trial runs. The study focused on the most optimal configuration, scenario 2, which incorporates a battery + SC HESS. The statistical parameters evaluated include the mean, SD, root mean square error (RMSE), and relative error (RE), providing a comprehensive understanding of the algorithm's consistency and reliability. Table 10 summarises these statistical metrics for the enhanced PSO algorithm, where N represents the number of independent trials. The descriptive statistics collectively indicate that the enhanced PSO algorithm exhibits low sensitivity to initial conditions and delivers robust performance. This suggests that a single execution of the algorithm is likely to yield an acceptable solution, making it practical for real-world applications. Minor variations in carbon footprint observed across different trials suggest that intermittent operation of the diesel generator may introduce slight instability in the total discounted lifecycle cost of the microgrid. However, these deviations remain within acceptable limits, further supporting the reliability of the proposed optimisation approach.

6.2. Performance analysis of the cycle counting algorithm for ESS

To evaluate the efficiency, effectiveness, and robustness of the proposed cycle counting algorithm for ESS, statistical analysis was conducted on the results from 40 independent optimisation trials. The analysis focused on the most optimal configuration, scenario 2, which incorporates a battery + SC HESS, and considered key output parameters, specifically the estimated lifetimes of the battery and SC. For comparison, an additional set of 40 independent trials was conducted using the same optimisation framework, but with the widely used rainflow counting algorithm applied for battery degradation modelling [105]. Statistical analysis was performed on the results of both methods, and the outcomes are summarized in Table 11. In addition to performance metrics, computational efficiency was assessed by comparing the overall runtime of the two algorithms in Table 12 below. The results demonstrate the proposed cycle counting method's advantages in both accuracy and computational speed, highlighting its suitability for lifecycle-based optimisation of standalone DC microgrids.

Table 12
Computational performance comparison of the proposed ESS degradation quantification algorithm with Rainflow counting algorithm.

ESS Degradation Algorithm	Average CPU Usage Time until convergence for Optimisation Problem (s)	Average No. of Iterations for Convergence	Average CPU Usage Time for one iteration (s)
Proposed ESS Degradation Quantification Algorithm (This Study)	6310	93	67.84
Rainflow Counting Algorithm	6442	94	68.53

Based on the results presented in Tables 11 and 12, it is evident that the proposed ESS degradation algorithm significantly outperforms the widely used rainflow counting algorithm in terms of both robustness and computational efficiency. This superior performance can be attributed to the algorithm's tailored design, which specifically addresses the degradation characteristics of ESS in standalone DC microgrid applications. Standalone microgrids often experience numerous partial charge-discharge cycles due to fluctuating renewable energy inputs and dynamic load profiles. The proposed algorithm accurately identifies and quantifies these partial cycles, leading to a more precise estimation of total cycle counts and degradation. In contrast, the rainflow counting algorithm, originally developed for fatigue analysis in mechanical systems, is less effective in capturing partial cycles in ESS operation. This limitation results in less accurate degradation modelling and higher variability in lifecycle cost predictions. The enhanced accuracy and efficiency of the proposed algorithm make it a more suitable choice for lifecycle cost optimisation of ESS in standalone DC microgrids.

7. Future research directions

Although this study provides valuable insights into the design of standalone DC microgrids for offshore applications, several assumptions were made that may affect the generalizability and accuracy of the results. In the hydrogen ESS, a fixed efficiency was assumed for the fuel cell. However, in real-world conditions, this efficiency may vary depending on operating voltage and current, ambient temperature, and atmospheric pressure. Future studies should investigate the impact of these dynamic parameters to enhance design accuracy, particularly for applications involving critical equipment. Additionally, the cost of hydrogen compression was assumed to be fixed, based on a final pressure of 700 bar, which is suitable for fuel cell vehicles [106]. However, different applications such as hydrogen-powered vessels, hydrogen turbines, and heating systems may require varying pressure levels. Future research should focus on tailoring hydrogen compression costs and pressure requirements to specific offshore applications.

In the probabilistic analysis, uncertainties in input parameters such as solar irradiance, wind speed, ambient temperature, and load demand were considered. However, uncertainties related to economic parameters, including fuel costs, ESS replacement costs, and operation and maintenance costs of RES and ESS, were not included. Incorporating these uncertainties would improve the robustness of the probabilistic design framework. To achieve this, multivariate joint distribution-based statistical methods can be employed. Copula-based techniques offer a viable and computationally efficient approach for modelling complex dependencies among uncertain variables [107].

To enable practical implementation of the proposed standalone DC microgrid design, its resiliency under extreme conditions, such as severe weather events and equipment faults, must be thoroughly investigated. Fault detection, handling, and clearance mechanisms should be thoroughly studied to enhance the system's robustness and reliability [108]. Future research should focus on developing strategies for managing these extreme scenarios to improve overall microgrid performance. Additionally, ancillary services such as black start capability are critical, especially in situations involving outages of fossil fuel-powered generators. Evaluating the microgrid's ability to restore operation under such conditions autonomously is essential for assessing its resiliency. Future studies should explore the integration of black start functionality and other ancillary services to ensure reliable operation in offshore and remote environments.

In this design, equipment degradation caused by harsh offshore conditions, such as corrosion due to salinity, was not considered. However, in practical implementations, such degradation can influence the lifecycle cost by increasing replacement frequency. Future studies should therefore focus on modelling equipment degradation under adverse environmental conditions and evaluating its impact on the design and economic feasibility of standalone DC microgrids.

8. Conclusion

Offshore standalone microgrids integrated with hydrogen fuel stations present a sustainable energy solution for powering maritime industries. HESS offer a cost-effective approach to managing the variability and uncertainty associated with RES in such applications. This manuscript introduces a novel meta-heuristic optimisation-based probabilistic model for designing a standalone DC microgrid with an integrated hydrogen fuel station, tailored explicitly for offshore industrial use. A case study involving a proposed aquaculture farm in New Zealand demonstrates the model's practical applicability and quantifiable outcomes.

The findings indicate that a battery + SC HESS configuration is the most economically viable energy storage solution for offshore standalone microgrids. This configuration reduces lifecycle costs by over 11 % compared to a battery-only setup. It achieves a 42 % lower LCOE than the hydrogen + SC HESS configuration, despite the additional investment in hydrogen infrastructure. These cost savings are primarily attributed to the system's ability to smooth power fluctuations, thereby reducing operational stress and extending the lifespan of the BESS. In the deterministic scenario, the battery + SC HESS configuration achieves an LCOE of 19.63 US cents per kWh, outperforming conventional diesel generator-based systems commonly used in offshore settings. This result underscores the economic and environmental feasibility of sustainable power supply solutions for offshore industries. Additionally, the study reveals that, at current cost levels, achieving cost parity with the battery + SC HESS configuration would require a 70.7 % reduction in fuel cell prices without any efficiency improvements. However, if fuel cell efficiency increases to 75 %, the reduction of cost needed decreases slightly to 69.3 %.

Another notable finding is that wave energy is currently not economically viable for offshore standalone microgrids due to the high costs and low efficiency of wave energy converters. These limitations hinder its competitiveness as a power source. Nevertheless, given that wave energy technology is still in its early stages, future advancements and cost reductions could enhance its feasibility, particularly in offshore environments. The study also highlights the importance of probabilistic modelling in microgrid design. Deterministic models tend to underestimate lifecycle costs, especially under extreme scenarios. In the optimal battery + SC HESS configuration, deviations from deterministic results are 6.9 % in the best-case scenario and 13.0 % in the worst-case scenario, with even larger deviations observed in other configurations. The probabilistic model effectively captures these variances, aligning the design process more closely with real-world operating conditions.

The effectiveness of the proposed methodologies was evaluated and compared with commonly used techniques to assess performance. Across 40 independent trials, the proposed enhanced PSO algorithm demonstrated superior performance in minimising lifecycle costs compared to standard PSO, GA, and ACO. This improvement is attributed to the integration of quadratic interpolation and extended local search mechanisms. The enhanced PSO also achieved faster convergence with fewer iterations, despite slightly higher per-iteration computational time. Statistical analysis confirmed its robustness and reliability, with low sensitivity to initial conditions. Furthermore, the proposed cycle counting algorithm for ESS outperformed the traditional rainflow counting method in both accuracy and computational efficiency, particularly in modelling partial charge-discharge cycles. These advancements make the proposed methodologies highly effective for real-world microgrid design and lifecycle cost optimisation.

While the study provides valuable insights, it is constrained by certain assumptions. Future research should address uncertainties related to equipment costs, component lifetimes, and the impact of adverse weather conditions offshore. Further exploration into operational strategies, such as day-ahead storage scheduling, demand response optimisation, and ancillary service provision, is also recommended. Overall, this study demonstrates that standalone microgrids,

particularly those utilising HESS configurations, represent a technically and economically feasible solution for sustainable offshore energy systems. These findings contribute to the advancement of a sustainable blue economy.

CRediT authorship contribution statement

Hasith Jayasinghe: Writing – original draft, Visualization, Validation, Software, Resources, Project administration, Methodology, Investigation, Formal analysis, Data curation, Conceptualization. **Kosala Gunawardane:** Writing – review & editing, Supervision, Project administration, Methodology, Funding acquisition, Formal analysis, Conceptualization. **Md. Alamgir Hossain:** Writing – review & editing, Visualization, Validation, Supervision, Resources. **Ramon Zamora:** Writing – review & editing, Supervision, Project administration, Funding acquisition, Conceptualization. **Mark Anthony Preece:** Data curation, Formal analysis, Investigation, Resources, Validation, Writing – review & editing.

Declaration of Generative AI and AI-assisted technologies in the writing process

During the preparation of this work the authors used ChatGPT and Gemini in order to improve language and readability. After using these tools, the authors reviewed and edited the content as needed and take full responsibility for the content of the publication.

Declaration of competing interest

The authors declare that they have no known competing financial interests or personal relationships that could have appeared to influence the work reported in this paper.

Acknowledgements

The authors acknowledge the financial support of the Blue Economy Cooperative Research Centre, established and supported under the Australian Government's Cooperative Research Centers Program, grant number CRCXX000001. The authors also thank The New Zealand King Salmon Company Limited for providing data to support this research.

Data availability

Data will be made available on request.

References

[1] A. Karimi Saeidabadi, S. Soleymani, B. Mozafari, H. Mohammadnezhadshourkaei, Optimizing power supply scheduling for offshore stand-alone microgrids: a novel framework considering load and fuel procurement uncertainties, Int. Trans. Electr. Energy Syst. 2024 (1) (2024) 5933462, https://doi.org/10.1155/2024/5933462.

[2] T. Hasan, K. Emami, R. Shah, N.M.S. Hassan, V. Belokoskov, M. Ly, Techno-economic assessment of a hydrogen-based islanded microgrid in north-east, Energy Rep. 9 (2023) 3380–3396, https://doi.org/10.1016/j.egyr.2023.02.019.

[3] X. Lin, R. Zamora, Controls of hybrid energy storage systems in microgrids: Critical review, case study and future trends, J. Energy Storage 47 (2022) 103884, https://doi.org/10.1016/j.est.2021.103884.

[4] T.B. Nkwanyana, M.W. Siti, Z. Wang, I. Toudjeu, N.T. Mbungu, W. Mulumba, An assessment of hybrid-energy storage systems in the renewable environments, J. Energy Storage 72 (2023) 108307, https://doi.org/10.1016/j.est.2023.108307.

[5] A. Emrani, A. Berrada, A comprehensive review on techno-economic assessment of hybrid energy storage systems integrated with renewable energy, J. Energy Storage 84 (2024) 111010, https://doi.org/10.1016/j.est.2024.111010.

[6] N. Kumaresan, A. Rammohan, A comprehensive review on energy management strategies of hybrid energy storage systems for electric vehicles, J. Braz. Soc. Mech. Sci. Eng. 46 (3) (2024) 146, https://doi.org/10.1007/s40430-024-04736-x.

[7] T. Lu, X. Yi, J. Li, S. Wu, Collaborative planning of integrated hydrogen energy chain multi-energy systems: a review, Appl. Energy 393 (2025) 126019, https://doi.org/10.1016/j.apenergy.2025.126019.

[8] C.N. Dimitriadis, E.G. Tsimopoulos, M.C. Georgiadis, Optimization-based economic analysis of energy storage technologies in a coupled electricity and natural gas market, J. Energy Storage 58 (2023) 106332, https://doi.org/10.1016/j.est.2022.106332.

[9] X. Voulkopoulos, C.N. Dimitriadis, M.C. Georgiadis, Optimal scheduling of a RES – Electrolyzer aggregator in electricity, hydrogen and green certificates markets, Int. J. Hydrog. Energy 78 (2024) 1099–1107, https://doi.org/10.1016/j.ijhydene.2024.06.379.

[10] T. Boonraksa, W. Pinthurat, P. Wongdet, P. Boonraksa, B. Marungsri, B. Hredzak, Optimal capacity and cost analysis of hybrid energy storage system in standalone DC microgrid, IEEE Access 11 (2023) 65496–65506, https://doi.org/10.1109/ACCESS.2023.3289821.

[11] Y. Tang, Q. Xun, M. Liserre, H. Yang, Energy management of electric-hydrogen hybrid energy storage systems in photovoltaic microgrids, Int. J. Hydrog. Energy 80 (2024) 1–10, https://doi.org/10.1016/j.ijhydene.2024.07.017.

[12] B. Li, H. Wang, Z. Tan, Capacity optimization of hybrid energy storage system for flexible islanded microgrid based on real-time price-based demand response, Int. J. Electr. Power Energy Syst. 136 (2022) 107581, https://doi.org/10.1016/j.ijepes.2021.107581.

[13] S. Mohseni, A.C. Brent, Probabilistic sizing and scheduling co-optimisation of hybrid battery/super-capacitor energy storage systems in micro-grids, J. Energy Storage 73 (2023) 109172, https://doi.org/10.1016/j.est.2023.109172.

[14] P.N.D. Premadasa, D.P. Chandima, An innovative approach of optimizing size and cost of hybrid energy storage system with state of charge regulation for stand-alone direct current microgrids, J. Energy Storage 32 (2020) 101703, https://doi.org/10.1016/j.est.2020.101703.

[15] S. Mohammadi, A. Mohammadi, Stochastic scenario-based model and investigating size of battery energy storage and thermal energy storage for micro-grid, Int. J. Electr. Power Energy Syst. 61 (2014) 531–546, https://doi.org/10.1016/j.ijepes.2014.03.041.

[16] U. Akram, M. Khalid, S. Shafiq, An innovative hybrid wind-solar and battery-supercapacitor microgrid system—development and optimization, IEEE Access 5 (2017) 25897–25912, https://doi.org/10.1109/ACCESS.2017.2767618.

[17] W. Dong, Y. Li, J. Xiang, Optimal sizing of a stand-alone hybrid power system based on battery/hydrogen with an improved ant colony optimization, Energies 9 (10) (2016) 10, https://doi.org/10.3390/en9100785.

[18] P.K. Behera, M. Pattnaik, Design and real-time implementation of wind–photovoltaic driven low voltage direct current microgrid integrated with hybrid energy storage system, J. Power Sources 595 (2024) 234028, https://doi.org/10.1016/j.jpowsour.2023.234028.

[19] P. Yegon and M. Singh, "Optimization of battery/ultra-capacitor hybrid energy storage system for frequency response support in low-inertia microgrid," IET Power Electron., vol. n/a, no. n/a, doi:https://doi.org/10.1049/pel2.12723.

[20] H. Chen, Z. Zhang, C. Guan, H. Gao, Optimization of sizing and frequency control in battery/supercapacitor hybrid energy storage system for fuel cell ship, Energy 197 (2020) 117285, https://doi.org/10.1016/j.energy.2020.117285.

[21] A. Abdelkader, A. Rabeh, D. Mohamed Ali, J. Mohamed, Multi-objective genetic algorithm based sizing optimization of a stand-alone wind/PV power supply system with enhanced battery/supercapacitor hybrid energy storage, Energy 163 (2018) 351–363, https://doi.org/10.1016/j.energy.2018.08.135.

[22] R.A. Younis, E. Touti, M. Aoudia, W. Zahrouni, A.I. Omar, A.H. Elmetwaly, Innovative hybrid energy storage systems with sustainable integration of green hydrogen and energy management solutions for standalone PV microgrids based on reduced fractional gradient descent algorithm, Res. Eng. Des. 24 (2024) 103229, https://doi.org/10.1016/j.rineng.2024.103229.

[23] A. Alzahrani, et al., Optimum sizing of stand-alone microgrids: Wind turbine, solar photovoltaic, and energy storage system, J. Energy Storage 73 (2023) 108611, https://doi.org/10.1016/j.est.2023.108611.

[24] T. Costa, et al., Development of a method for sizing a hybrid battery energy storage system for application in AC microgrid, Energies 16 (3) (2023) 3, https://doi.org/10.3390/en16031175.

[25] D. Wang, M. Grimmelt, Climate influence on the optimal stand-alone microgrid system with hybrid storage – a comparative study, Renew. Energy 208 (2023) 657–664, https://doi.org/10.1016/j.renene.2023.03.045.

[26] L. Al-Ghussain, A. Darwish Ahmad, A.M. Abubaker, M.A. Mohamed, An integrated photovoltaic/wind/biomass and hybrid energy storage systems towards 100% renewable energy microgrids in university campuses, Sustain. Energy Technol. Assess. 46 (2021) 101273, https://doi.org/10.1016/j.seta.2021.101273.

[27] M.F. Elmorshedy, M.R. Elkadeem, K.M. Kotb, I.B.M. Taha, D. Mazzeo, Optimal design and energy management of an isolated fully renewable energy system integrating batteries and supercapacitors, Energy Convers. Manag. 245 (2021) 114584, https://doi.org/10.1016/j.enconman.2021.114584.

[28] K.J. Lim, L.W. Chong, S. Morris, B.H. Lim, M. Fahmi, C. Palanichamy, "Battery Lifetime And Life Cycle Cost Analysis Of Battery-Supercapacitor Hybrid Energy Storage System For Standalone Power System," in 2022 IEEE 5th International Symposium in Robotics and Manufacturing Automation (ROMA), 2022, pp. 1–6, https://doi.org/10.1109/ROMA55875.2022.9915663.

[29] Y. Belkhier, A. Oubelaid, Novel design and adaptive coordinated energy management of hybrid fuel-cells/tidal/wind/PV array energy systems with battery storage for microgrids, Energy Storage 6 (1) (2024) e556, https://doi.org/10.1002/est2.556.

[30] M.F. Diabate, H. Krishnamoorthy, J. Shi, Optimal design and modeling of a hybrid energy storage system including battery and hydrogen in DC microgrids, IEEE Trans. Ind. Appl. (2025) 1–13, https://doi.org/10.1109/TIA.2025.3554127.

[31] B. Du, et al., Compatible matching and synergy operation optimization of hydrogen-electric hybrid energy storage system in DC microgrid, Energ. Convers. Manag. X 26 (2025) 101014, https://doi.org/10.1016/j.ecmx.2025.101014.
[32] X. Xie, X. Quan, Z. Wu, F. Zeng, H. Miu, X. Yuan, Optimizing AC/DC microgrid scheduling with electro-hydrogen hybrid energy storage for low-carbon buildings, Int. J. Hydrog. Energy 143 (2025) 716–727, https://doi.org/10.1016/j.ijhydene.2025.05.016.
[33] M.A. Hossain, H.R. Pota, S. Squartini, A.F. Abdou, Modified PSO algorithm for real-time energy management in grid-connected microgrids, Renew. Energy 136 (2019) 746–757, https://doi.org/10.1016/j.renene.2019.01.005.
[34] H. Yang, C. Zhang, J. Li, L. Zhu, K. Zhou, A novel robust energy storage planning method for grids with wind power integration considering the impact of hurricanes, IEEE Trans. Sustain. Energy 16 (2) (2025) 1388–1400, https://doi.org/10.1109/TSTE.2025.3527448.
[35] P. Wang, R. Xiong, W. Shen, F. Sun, Aging-induced, rate-independent lithium plating: a complete mechanism analysis throughout the battery lifecycle, Appl. Energy 393 (2025) 126094, https://doi.org/10.1016/j.apenergy.2025.126094.
[36] Z.M. Ali, M. Calasan, S.H.E.A. Aleem, F. Jurado, F.H. Gandoman, Applications of energy storage systems in enhancing energy management and access in microgrids: A review, Energies 16 (16) (2023) 16, https://doi.org/10.3390/en16165930.
[37] T.E.K. Zidane, et al., Grid-connected solar PV power plants optimization: a review, IEEE Access 11 (2023) 79588–79608, https://doi.org/10.1109/ACCESS.2023.3299815.
[38] A. Ameur, A. Berrada, K. Loudiyi, M. Aggour, Forecast modeling and performance assessment of solar PV systems, J. Clean. Prod. 267 (2020) 122167, https://doi.org/10.1016/j.jclepro.2020.122167.
[39] L.A. Fernandez-Jimenez, C. Monteiro, I.J. Ramirez-Rosado, Short-term probabilistic forecasting models using Beta distributions for photovoltaic plants, Energy Rep. 9 (2023) 495–502, https://doi.org/10.1016/j.egyr.2023.01.059.
[40] A. Wan, et al., Robust loop shaping design pitch control of wind turbine for maximal power output and reduced loading, Energy 319 (2025) 135136, https://doi.org/10.1016/j.energy.2025.135136.
[41] H. Jayasinghe, K. Gunawardane, R. Zamora, Multi-objective optimisation framework for standalone DC-microgrids with direct load control in demand-side management, Electron. Lett. 60 (15) (2024) e13290, https://doi.org/10.1049/ell2.13290.
[42] M. Yang, R. Jiang, X. Yu, B. Wang, X. Su, C. Ma, Extraction and application of intrinsic predictable component in day-ahead power prediction for wind farm cluster, Energy 328 (2025) 136530, https://doi.org/10.1016/j.energy.2025.136530.
[43] J. Orszaghova, et al., Variability of wave power production of the M4 machine at two energetic open ocean locations: Off Albany, Western Australia and at EMEC, Orkney, UK, Renew. Energy 197 (2022) 417–431, https://doi.org/10.1016/j.renene.2022.07.053.
[44] G. Zhang, W. Wang, J. Du, H. Sheng, Multiobjective economic optimal dispatch for the island isolated microgrid under uncertainty based on interval optimization, Math. Probl. Eng. 2021 (1) (2021) 9983104, https://doi.org/10.1155/2021/9983104.
[45] B. Guo, J.V. Ringwood, A review of wave energy technology from a research and commercial perspective, IET Renew. Power Gener. 15 (14) (2021) 3065–3090, https://doi.org/10.1049/rpg2.12302.
[46] B. Yang, et al., A critical survey of power take-off systems based wave energy converters: summaries, advances, and perspectives, Ocean Eng. 298 (2024) 117149, https://doi.org/10.1016/j.oceaneng.2024.117149.
[47] J. Marqusee, S. Ericson, D. Jenket, Impact of emergency diesel generator reliability on microgrids and building-tied systems, Appl. Energy 285 (2021) 116437, https://doi.org/10.1016/j.apenergy.2021.116437.
[48] U. Manandhar, X. Zhang, G.H. Beng, L. Subramanian, H.H.C. Lu, T. Fernando, Enhanced energy management system for isolated microgrid with diesel generators, renewable generation, and energy storages, Appl. Energy 350 (2023) 121624, https://doi.org/10.1016/j.apenergy.2023.121624.
[49] S. Makhdoomi, A. Askarzadeh, Optimizing operation of a photovoltaic/diesel generator hybrid energy system with pumped hydro storage by a modified crow search algorithm, J. Energy Storage 27 (2020) 101040, https://doi.org/10.1016/j.est.2019.101040.
[50] P.N.D. Premadasa, C.M.M.R.S. Silva, D.P. Chandima, J.P. Karunadasa, A multi-objective optimization model for sizing an off-grid hybrid energy microgrid with optimal dispatching of a diesel generator, J. Energy Storage 68 (2023) 107621, https://doi.org/10.1016/j.est.2023.107621.
[51] L. Zhao, et al., Prussian blue analogues for advanced non-aqueous sodium ion batteries: Redox mechanisms, key challenges and modification strategies, Energy Storage Mater. 78 (2025) 104256, https://doi.org/10.1016/j.ensm.2025.104256.
[52] M. Gholami, S.A. Mousavi, S.M. Muyeen, Enhanced microgrid reliability through optimal battery Energy storage system type and sizing, IEEE Access 11 (2023) 62733–62743, https://doi.org/10.1109/ACCESS.2023.3288427.
[53] J.J. Caparrós Mancera, et al., Experimental analysis of the effects of supercapacitor banks in a renewable DC microgrid, Appl. Energy 308 (2022) 118355, https://doi.org/10.1016/j.apenergy.2021.118355.
[54] A.H. Tariq, S.A.A. Kazmi, M. Hassan, S.A. Muhammed Ali, M. Anwar, Analysis of fuel cell integration with hybrid microgrid systems for clean energy:a comparative review, Int. J. Hydrog. Energy 52 (2024) 1005–1034, https://doi.org/10.1016/j.ijhydene.2023.07.238.
[55] D. Yousri, R.H. AlKuwaiti, H.E.Z. Farag, H. Zeineldin, E. El-Saadany, Advanced modeling of PEM electrolyzers for microgrid systems: Incorporating electrochemical and thermal models, Int. J. Hydrog. Energy 83 (2024) 755–773, https://doi.org/10.1016/j.ijhydene.2024.08.023.
[56] L. Valverde, F. Rosa, C. Bordons, Design, planning and management of a hydrogen-based microgrid, IEEE Trans. Ind. Inform. 9 (3) (2013) 1398–1404, https://doi.org/10.1109/TII.2013.2246576.
[57] Q. Rong, P. Hu, Y. Yu, D. Wang, Y. Cao, H. Xin, Virtual external perturbance-based impedance measurement of grid-connected converter, IEEE Trans. Ind. Electron. 72 (3) (2025) 2644–2654, https://doi.org/10.1109/TIE.2024.3436629.
[58] N. Li, et al., Single-degree-of-freedom hybrid modulation strategy and light-load efficiency optimization for dual-active-bridge converter, IEEE J. Emerg. Sel. Top. Power Electron. 12 (4) (2024) 3936–3947, https://doi.org/10.1109/JESTPE.2024.3396340.
[59] J. Zhang, et al., A novel multiple-medium-AC-port power electronic transformer, IEEE Trans. Ind. Electron. 71 (7) (2024) 6568–6578, https://doi.org/10.1109/TIE.2023.3301550.
[60] A.C. Nanakos, E.C. Tatakis, N.P. Papanikolaou, A weighted-efficiency-oriented design methodology of Flyback inverter for AC photovoltaic modules, IEEE Trans. Power Electron. 27 (7) (2012) 3221–3233, https://doi.org/10.1109/TPEL.2011.2182211.
[61] OECD, Effective Carbon Rates 2023, 2023, https://doi.org/10.1787/b84d5b36-en.
[62] X. Ding, H. Ma, Z. Yan, J. Xing, J. Sun, Distributionally robust capacity configuration for energy storage in microgrid considering renewable utilization, Front. Energy Res. 10 (2022), https://doi.org/10.3389/fenrg.2022.923985.
[63] D. Ray, Lazard's Levelized Cost of Energy Analysis—Version 13.0, 2020.
[64] L. Xu, X. Ruan, C. Mao, B. Zhang, Y. Luo, An improved optimal sizing method for wind-solar-battery hybrid power system, IEEE Trans. Sustain. Energy 4 (3) (2013) 774–785, https://doi.org/10.1109/TSTE.2012.2228509.
[65] S. Mandava, A. Gudipalli, N. Amutha Prabha, G.K. Rajini, Control of micro-grid by discretized PR controller using Tustin frequency pre-wrapping method, in: V.L. N. Komanapalli, N. Sivakumaran, S. Hampannavar (Eds.), Advances in Automation, Signal Processing, Instrumentation, and Control, Springer Nature, Singapore, 2021, pp. 2301–2311, https://doi.org/10.1007/978-981-15-8221-9_215.
[66] N. Padmawansa, K. Gunawardane, K. Subasinghage, "Fuel Cell and Supercapacitor Hybrid Energy Storage for Regulating DC Link Voltage in DC Microgrids," in 2024 IEEE 9th Southern Power Electronics Conference (SPEC), 2024, pp. 1–6, https://doi.org/10.1109/SPEC62217.2024.10892815.
[67] S. Li, H. He, C. Su, P. Zhao, Data driven battery modeling and management method with aging phenomenon considered, Appl. Energy 275 (2020) 115340, https://doi.org/10.1016/j.apenergy.2020.115340.
[68] J.-O. Lee, Y.-S. Kim, Novel battery degradation cost formulation for optimal scheduling of battery energy storage systems, Int. J. Electr. Power Energy Syst. 137 (2022) 107795, https://doi.org/10.1016/j.ijepes.2021.107795.
[69] Obtaining climate data from NIWA | NIWA, Accessed: Oct. 15, 2024. [Online]. Available: https://niwa.co.nz/climate-and-weather/obtaining-climate-data-niwa.
[70] M. Rahmani-Andebili, M. Bonamente, J.A. Miller, Charging management of plug-in electric vehicles in San Francisco applying Monte Carlo Markov chain and stochastic model predictive control and considering renewables and drag force, IET Gener. Transm. Distrib. 14 (25) (2020) 6179–6188, https://doi.org/10.1049/iet-gtd.2020.1106.
[71] R. Karuppiah, M. Martín, I.E. Grossmann, A simple heuristic for reducing the number of scenarios in two-stage stochastic programming, Comput. Chem. Eng. 34 (8) (2010) 1246–1255, https://doi.org/10.1016/j.compchemeng.2009.10.009.
[72] A. SoltaniNejad Farsangi, S. Hadayeghparast, M. Mehdinejad, H. Shayanfar, A novel stochastic energy management of a microgrid with various types of distributed energy resources in presence of demand response programs, Energy 160 (2018) 257–274, https://doi.org/10.1016/j.energy.2018.06.136.
[73] A. Quteishat, M.A. Younis, A. Safari, A. Jahangiri, A fuzzy cloud theory-based stochastic model for multi-carrier energy hubs in grid-connected and islanded operations, Electr. Eng. 107 (1) (2025) 929–945, https://doi.org/10.1007/s00202-024-02555-w.
[74] S. Mohseni, R. Khalid, A.C. Brent, Stochastic, resilience-oriented optimal sizing of off-grid microgrids considering EV-charging demand response: an efficiency comparison of state-of-the-art metaheuristics, Appl. Energy 341 (2023) 121007, https://doi.org/10.1016/j.apenergy.2023.121007.
[75] M.R. AlRashidi, M.E. El-Hawary, A survey of particle swarm optimization applications in electric power systems, IEEE Trans. Evol. Comput. 13 (4) (2009) 913–918, https://doi.org/10.1109/TEVC.2006.880326.
[76] W. Assawinchaichote, C. Angeli, J. Pongfai, Proportional-integral-derivative parametric autotuning by Novel Stable Particle Swarm Optimization (NSPSO), IEEE Access 10 (2022) 40818–40828, https://doi.org/10.1109/ACCESS.2022.3167026.
[77] S. Tiwari, A. Kumar, Advances and bibliographic analysis of particle swarm optimization applications in electrical power system: concepts and variants, Evol. Intell. 16 (1) (2023) 23–47, https://doi.org/10.1007/s12065-021-00661-3.
[78] M.A. Hossain, R.K. Chakrabortty, M.J. Ryan, H.R. Pota, Energy management of community energy storage in grid-connected microgrid under uncertain real-time prices, Sustain. Cities Soc. 66 (2021) 102658, https://doi.org/10.1016/j.scs.2020.102658.
[79] G. Papazoglou, P. Biskas, Review and comparison of genetic algorithm and particle swarm optimization in the optimal power flow problem, Energies 16 (3) (2023) 3, https://doi.org/10.3390/en16031152.
[80] M. Qaraad, S. Amjad, N.K. Hussein, M.A. Farag, S. Mirjalili, M.A. Elhosseini, Quadratic interpolation and a new local search approach to improve particle

swarm optimization: Solar photovoltaic parameter estimation, Expert Syst. Appl. 236 (2024) 121417, https://doi.org/10.1016/j.eswa.2023.121417.
[81] Blue Economy CRC | Underpinning the Growth of the Blue Economy, Blue Economy Cooperative Research Centre, Accessed: Jul. 14, 2025. [Online]. Available: https://blueeconomycrc.com.au/.
[82] D. Carrasco-Bahamonde, A. Casellas, Evolving blue development discourses and policies: Salmon farming industry and regional making in Chile, Mar. Policy 163 (2024) 106111, https://doi.org/10.1016/j.marpol.2024.106111.
[83] Open Ocean – Blue Endeavour – New Zealand King Salmon, Accessed: Oct. 15, 2024. [Online]. Available: https://www.kingsalmon.co.nz/open-ocean-blue-endeavour/.
[84] Learn about SunPower Solar Panels | SunPower, Accessed: Sep. 20, 2024. [Online]. Available: https://us.sunpower.com/products/solar-panels.
[85] A. Pecher, J.P. Kofoed, T. Larsen, Design specifications for the Hanstholm WEPTOS wave energy converter, Energies 5 (4) (2012) 4, https://doi.org/10.3390/en5041001.
[86] Argolabe Engineering | Catia V5, Siemens NX, Projects and Consulting, Accessed: Sep. 20, 2024. [Online]. Available: https://www.argolabe.es/.
[87] M.A. Hossain, H.R. Pota, S. Squartini, F. Zaman, K.M. Muttaqi, Energy management of community microgrids considering degradation cost of battery, J. Energy Storage 22 (2019) 257–269, https://doi.org/10.1016/j.est.2018.12.021.
[88] B. Liu, et al., State of charge estimation of supercapacitor under different temperatures using particle filter algorithm based on fractional-order model, J. Electrochem. Soc. 170 (9) (2023) 090541, https://doi.org/10.1149/1945-7111/acfac3.
[89] Fuel Cells, Energy.gov, Accessed: Sep. 20, 2024. [Online]. Available: https://www.energy.gov/eere/fuelcells/fuel-cells.
[90] Z. Ding, D. Ning, R. Mayon, Wave-to-wire model for an oscillating water column wave energy converter, Appl. Energy 377 (2025) 124663, https://doi.org/10.1016/j.apenergy.2024.124663.
[91] T. Wang, X. Cao, L. Jiao, PEM water electrolysis for hydrogen production: Fundamentals, advances, and prospects, Carbon Neutrality 1 (1) (2022) 21, https://doi.org/10.1007/s43979-022-00022-8.
[92] E.T.S. Inc, U.S.D. Energy, Fuel Cell Handbook *(Seventh Edition)*. Lulu.com [Online]. Available: https://books.google.com.au/books?id=S9GZDAEACAAJ, 2016.
[93] H. Zhang, S. Su, G. Lin, J. Chen, Efficiency calculation and configuration design of a PEM electrolyzer system for hydrogen production, Int. J. Electrochem. Sci. 7 (5) (2012) 4143–4157, https://doi.org/10.1016/S1452-3981(23)19527-7.
[94] R. Khajuria, S. Yelisetti, R. Lamba, R. Kumar, Optimal model parameter estimation and performance analysis of PEM electrolyzer using modified honey badger algorithm, Int. J. Hydrog. Energy 49 (2024) 238–259, https://doi.org/10.1016/j.ijhydene.2023.07.172.
[95] Annual Energy Outlook 2023 - U.S. Energy Information Administration (EIA), Accessed: Sep. 20, 2024. [Online]. Available: https://www.eia.gov/outlooks/aeo/index.php.
[96] C. Guo, W. Sheng, D.G. De Silva, G. Aggidis, A review of the levelized cost of wave energy based on a techno-economic model, Energies 16 (5) (2023) 5, https://doi.org/10.3390/en16052144.
[97] S. Link, A. Stephan, D. Speth, P. Plötz, Rapidly declining costs of truck batteries and fuel cells enable large-scale road freight electrification, Nat. Energy 9 (8) (2024) 1032–1039, https://doi.org/10.1038/s41560-024-01531-9.
[98] A. Farhadi, M.T. Iqbal, Optimal sizing and techno-economic analysis of a hybrid power system for Postville, Eur. J. Eng. Technol. Res. 9 (2) (2024) 2, https://doi.org/10.24018/ejeng.2024.9.2.3127.
[99] A. Badgett, et al., Updated Manufactured Cost Analysis for Proton Exchange Membrane Water Electrolyzers, 2024, https://doi.org/10.2172/2311140.
[100] K.B. Samal, S. Pati, R. Sharma, A review of FCs integration with microgrid and their control strategies, Int. J. Hydrog. Energy 48 (91) (2023) 35661–35684, https://doi.org/10.1016/j.ijhydene.2023.05.287.
[101] H.-A. Trinh, H.V.A. Truong, M.D. Pham, T.C. Do, H.-H. Lee, K.K. Ahn, Comprehensive control strategy and verification for PEM fuel cell/battery/supercapacitor hybrid power source, Int. J. Precis. Eng. Manuf.-Green Technol. 10 (2) (2023) 421–436, https://doi.org/10.1007/s40684-022-00498-w.
[102] J.M. Weinand, et al., Global LCOEs of decentralized off-grid renewable energy systems, Renew. Sust. Energ. Rev. 183 (2023) 113478, https://doi.org/10.1016/j.rser.2023.113478.
[103] S.-F. Wang, H.-P. Chen, Y. Ku, M.-X. Zhong, Analytical synthesis of high-pass, band-pass and low-pass biquadratic filters and its quadrature oscillator application using current-feedback operational amplifiers, IEEE Access 9 (2021) 13330–13343, https://doi.org/10.1109/ACCESS.2021.3050751.
[104] H. Schmidt, G. Thierauf, A combined heuristic optimization technique, Adv. Eng. Softw. 36 (1) (2005) 11–19, https://doi.org/10.1016/j.advengsoft.2003.12.001.
[105] M.J.E. Alam, T.K. Saha, Cycle-life degradation assessment of Battery Energy Storage Systems caused by solar PV variability, in: 2016 IEEE Power and Energy Society General Meeting (PESGM), 2016, pp. 1–5, https://doi.org/10.1109/PESGM.2016.7741532.
[106] G. Singer, R. Köll, L. Aichhorn, P. Pertl, A. Trattner, Utilizing hydrogen pressure energy by expansion machines – PEM fuel cells in mobile and other potential applications, Appl. Energy 343 (2023) 121056, https://doi.org/10.1016/j.apenergy.2023.121056.
[107] Z. Shi, J. Chen, Y. Wang, Y. Zhao, B. Xu, Credibility copula-based robust multistage plan for industrial parks under exogenous and endogenous uncertainties, CSEE J. Power Energy Syst. 11 (3) (2025) 987–998, https://doi.org/10.17775/CSEEJPES.2024.09120.
[108] K. Wang, et al., A coordinated reconfiguration strategy for multi-stage resilience enhancement in integrated power distribution and heating networks, IEEE Trans. Smart Grid 14 (4) (2023) 2709–2722, https://doi.org/10.1109/TSG.2022.3231590.